A Trojan horse approach for enhancing the cellular uptake of a ruthenium nitrosyl complex

Pablo Labra-Vázquez, Erika Rocha, Yue Xiao, Marine Tassé, Carine Duhayon, Norberto Farfán, Rosa Santillan, Laure Gibot, Pascal Lacroix, Isabelle Malfant

View Article Online
View Journal

Dalton Transactions

An international journal of inorganic chemistry

Accepted Manuscript

This article can be cited before page numbers have been issued, to do this please use: P. Labra-Vázquez, E. Rocha, Y. Xiao, M. Tassé, C. Duhayon, N. Farfán, R. Santillan, L. Gibot, P. G. Lacroix and I. Malfant, *Dalton Trans.*, 2023, DOI: 10.1039/D3DT03480A.

ROYAL SOCIETY OF CHEMISTRY

rsc.li/dalton

View Article Online
DOI: 10.1039/D3DT03480A

A Trojan Horse Approach to Enhancing the Cell Income of a Ruthenium Nitrosyl Complex

Pablo Labra-Vázquez[a,b,*], Erika Rocha[b], Yue Xiao[a], Marine Tassé[a], Carine Duhayon[a], Norberto Farfán[b,*], Rosa Santillan[c], Laure Gibot[d], Pascal G. Lacroix[a], Isabelle Malfant[a,*]

[a]*Laboratoire de Chimie de Coordination du CNRS, 205 route de Narbonne, F-31077, Toulouse, France.*
[b]*Facultad de Química, Departamento de Química Orgánica, Universidad Nacional Autónoma de México, Ciudad Universitaria, 04510 Ciudad de México, México*
[c]*Departamento de Química, Centro de Investigación y de Estudios Avanzados del IPN, Apdo. Postal 14-740, 07000, Ciudad de México, México.*
[d]*Laboratoire Softmat, Université de Toulouse, CNRS UMR 5623, Université Toulouse III – Paul Sabatier*
*****Corresponding authors. E-mail addresses:* pab.labra@gmail.com, norberto.farfan@gmail.com, *isabelle.malfant@lcc-toulouse.fr*

Abstract

Ruthenium nitrosyl (RuNO) complexes continue to attract significant research interest due to several appealing features that make these photoactivatable nitric oxide (NO·) donors attractive for applications in photoactivated chemotherapy. Interesting examples of molecular candidates capable of delivering cytotoxic concentrations of NO· in aqueous media have been informed. Nevertheless, the question of whether most of these highly polar and relatively large molecules are efficiently incorporated by cells remains largely unanswered. In this paper, we present the synthesis and the chemical, photophysical and photochemical characterization of RuNO complexes functionalized with 17α-ethinylestradiol (**EE**), a semisynthetic steroidal hormone intended to act as a molecular Trojan horse for the targeted delivery of RuNO complexes. The discussion is centered around two main molecular targets, one containing **EE** (**EE-Phtpy-RuNO**) and a reference compound lacking this biological recognition fragment (**Phtpy-RuNO**). While both complexes displayed similar optical absorption profiles and NO· release efficiencies in aqueous media, important differences were found regarding their cellular uptake towards dermal fibroblasts, with **EE-Phtpy-RuNO** gratifyingly displaying a remarkable 10-fold increase in cell uptake when compared to **Phtpy-RuNO**, thus demonstrating the potential drug-targeting capabilities of this biomimetic steroidal conjugate.

View Article Online
DOI: 10.1039/D3DT03480A

INTRODUCTION

With cancer remaining as one of the leading causes of death worldwide,[1] significant research activity continues to be devoted to the challenging task of selectively and efficiently delivering drugs into tumor cells.[2-3] This has led to the development of diverse strategies that exploit the various processes involved in the transport of molecules into cells.[4-5] Physicochemical properties play a decisive role, with drugs featuring a good lipophilicity and a low molecular weight generally dissolving well in the phospholipids of the cellular membrane and thus penetrating efficiently into cells.[6] This relationship between physicochemical parameters and penetrating ability[7-9] leads to the possibility of tailoring a drug in order to enhance its cellular uptake. More sophisticated strategies include the development of nanoscale carriers[10] and the attachment of a biological recognition fragment[11-12] capable of interacting selectively with a specific cell membrane receptor,[13-15] easing the uptake of drugs not able to cross the cell membrane. Bypassing biological barriers using biomimetic drugs, often called molecular Trojan horses,[16-17] indeed enhances cellular uptake and accumulation of the drug into a specific tissue.[18-20]

This targeting strategy has not only been applied to 'classical' chemotherapeutics such as platinum complexes,[19, 21] but also in the context of next-generation light-triggered cancer therapies such as photoactivated chemotherapy (PACT).[22-25] PACT is based on the use of compounds that are poorly or negligibly cytotoxic except when irradiated with light, which triggers the photocleavage of the molecule and the generation of cytotoxic photoproducts.[26-27] As the use of PACT implies the local activation of cytotoxicity by light, nonilluminated tissues should normally remain undamaged. In this context, the introduction of a recognition fragment in photo-triggered therapies is aimed at improving its accumulation into the targeted tissue, avoiding toxicity on untargeted organs.[28-31] Ruthenium nitrosyl (RuNO) complexes lie among the most studied PACT agents; upon illumination, these complexes are capable of releasing nitric oxide (NO·), a small, endogenously-produced radical with important biological effects that are highly dependent on its concentration.[32-33] With high NO· concentrations leading to cell death, these phototherapeutic agents can potentially be applied for anticancer therapy, provided that the radical is effectively delivered in a controlled manner inside the malignant tissue.

Our research group has been actively involved in the development of RuNO complexes that can be activated using the two-photon absorption technique, which allows the efficient photorelease of NO· under near-infrared (NIR) excitation.[34-35] While significant advances have provided us with highly photoreactive systems that deliver biologically relevant amounts of NO·,[36-37] the question of whether such highly polar and relatively large molecules are efficiently incorporated by cells remains unanswered. In this context, we decided to investigate the influence of attaching a biological recognition fragment on the cellular uptake efficiency of a RuNO complex. For this purpose, we chose 17α-ethinylestradiol (**EE**), a semisynthetic steroidal contraceptive,[38] considering the significant evidence showing that cytotoxic steroidal conjugates are well carried through the blood and accumulate selectively into specific tissues.[39-40] More specifically, the introduction of **EE** allows targeting the estrogen receptors (ER), a family of membrane and nuclear receptors[41-43] present in a variety of human tissues, including the skin,[44] and overexpressed in the most common types of breast cancer.[31, 45] Targeting the ER in the context of cancer therapy has become so relevant that is considered today a paradigm in targeted therapy.[46]

View Article Online
DOI: 10.1039/D3DT03480A

Taking the previous into account, we hypothesized that attaching **EE** to a RuNO complex could result in (*i*) an enhanced cellular uptake efficiency and (*ii*) a selective accumulation of the complex in tissues where ER are overexpressed, such as breast cancer. To investigate the first expectation, in this paper we report an investigation on a group of steroidal RuNO complexes bearing **EE** as a biological recognition fragment. The structures of the investigated complexes are shown in Chart 1, all of which bear a terpyridyl ligand functionalized with **EE** (**EE-Phtpy**). The link between the RuNO moiety and the steroid occurs through the steroidal 5-membered D-ring following reports on unfavorable interactions with ER for alternative connectivities.[47] The ligand is employed in the obtention of a pair of *cis*(Cl,Cl)- and *trans*(Cl,Cl)-[Ru^{II}(**EE-Phtpy**)(NO)Cl_2](PF_6) isomeric complexes (***cis*-4a** and ***trans*-4a**, respectively) and of complex *trans*(NO,OH)-[Ru^{II}(**EE-Phtpy**)(NO)(OH)Cl](PF_6) (**EE-Phtpy-RuNO**), where one chlorido is replaced by a hydroxido ligand. Previous investigations have shown that complexes with the same coordination sphere of **EE-Phtpy-RuNO** are obtained as the water-stable product of the hydrolysis of dichloro-RuNO terpyridyl complexes (such as ***cis*-** and ***trans*-4a**).[36-37] We therefore considered **EE-Phtpy-RuNO** as the best candidate for the biological investigations.

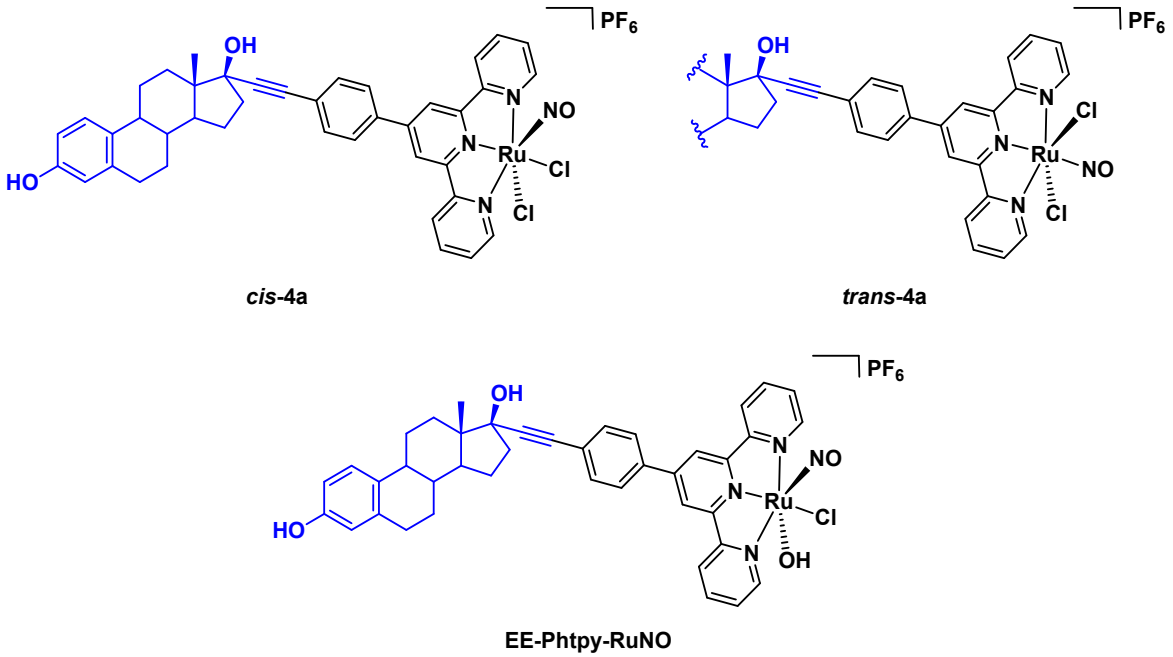

Chart 1. Steroidal ruthenium nitrosyl complexes under investigation. The 17α-ethinylestradiol (**EE**) fragment is shown in blue.

The manuscript is organized as follows: first, the synthesis and chemical characterization of ***cis*-4a** and ***trans*-4a** are presented, followed by an investigation of the hydrolysis towards **EE-Phtpy-RuNO** and the study of the optical absorption profiles of these complexes. Then, we conduct a structural analysis supported by single-crystal X-Ray diffraction (SXRD) and IR spectroscopy. A discussion of the NO-photorelease properties of the studied compounds is presented afterwards, followed by partition coefficient (logP) measurements and a biological study of their cellular uptake efficiency towards human dermal fibroblasts supported by inductively coupled plasma mass spectrometry (ICP-MS) measurements. To provide a clear understanding on the influence of the

View Article Online
DOI: 10.1039/D3DT03480A

attachment of **EE** on the photophysical, photochemical and biological properties of the target steroidal RuNO complexes, comparisons with reference complexes lacking the **EE** fragment are systematically presented.

RESULTS AND DISCUSSION

Synthesis and Characterization

The synthesis of the target steroidal ruthenium nitrosyl complexes ***cis*-** and ***trans*-4a** and of the reference complexes lacking the **EE** fragment (***cis*-** and ***trans*-4b**) was carried out following the multi-step synthesis shown in Scheme 1. The synthesis of the reference ligand (**2b**) and its complexes has already been informed elsewhere[48] and consequently will not be discussed in detail here. In the case of the steroidal derivatives, the synthesis started by the preparation of aldehyde **1a** which was obtained employing a Sonogashira cross-coupling reaction between **EE** and 4-bromobenzaldehyde, as reported elsewhere.[49] Then, aldehydes **1a-b** were subjected to a one-pot Kröhnke pyridine synthesis affording terpyridyl ligands **2a** (**EE-Phtpy**) and **2b** (**Phtpy**) being conveniently obtained following the methodology reported by J. Wang and G. S. Hanan[50] with minor modifications.

Ligands **2a-b** were subsequently subjected to metalation using $RuCl_3xH_2O$ yielding Ru^{III} complexes **3a-b**, which were finally dissolved in warm dimethylformamide and treated with $NO^{\cdot}$, generated by the reaction between copper and HNO_3. This procedure yielded analytical samples of the desired ***cis*-4a-b** and ***trans*-4a-b** ruthenium nitrosyl complexes after HPLC purification followed by metathesis using aqueous NH_4PF_6. It should be noted that, before purification, this last step systematically yields a crude product containing both isomeric ruthenium nitrosyl complexes and varying amounts of the corresponding Ru^{II} bis-terpyridyl homoleptic species,[37] which is not systematically isolated. IR and MS analyses on the crude product (See Supplementary Figures S3-S4) evidenced a similar outcome in the present case, with the steroidal homoleptic complex, Ru^{II}(**EE-Phtpy**)$_2$(PF_6)$_2$, being isolated and characterized along with the desired RuNO complexes.

View Article Online
DOI: 10.1039/D3DT03480A

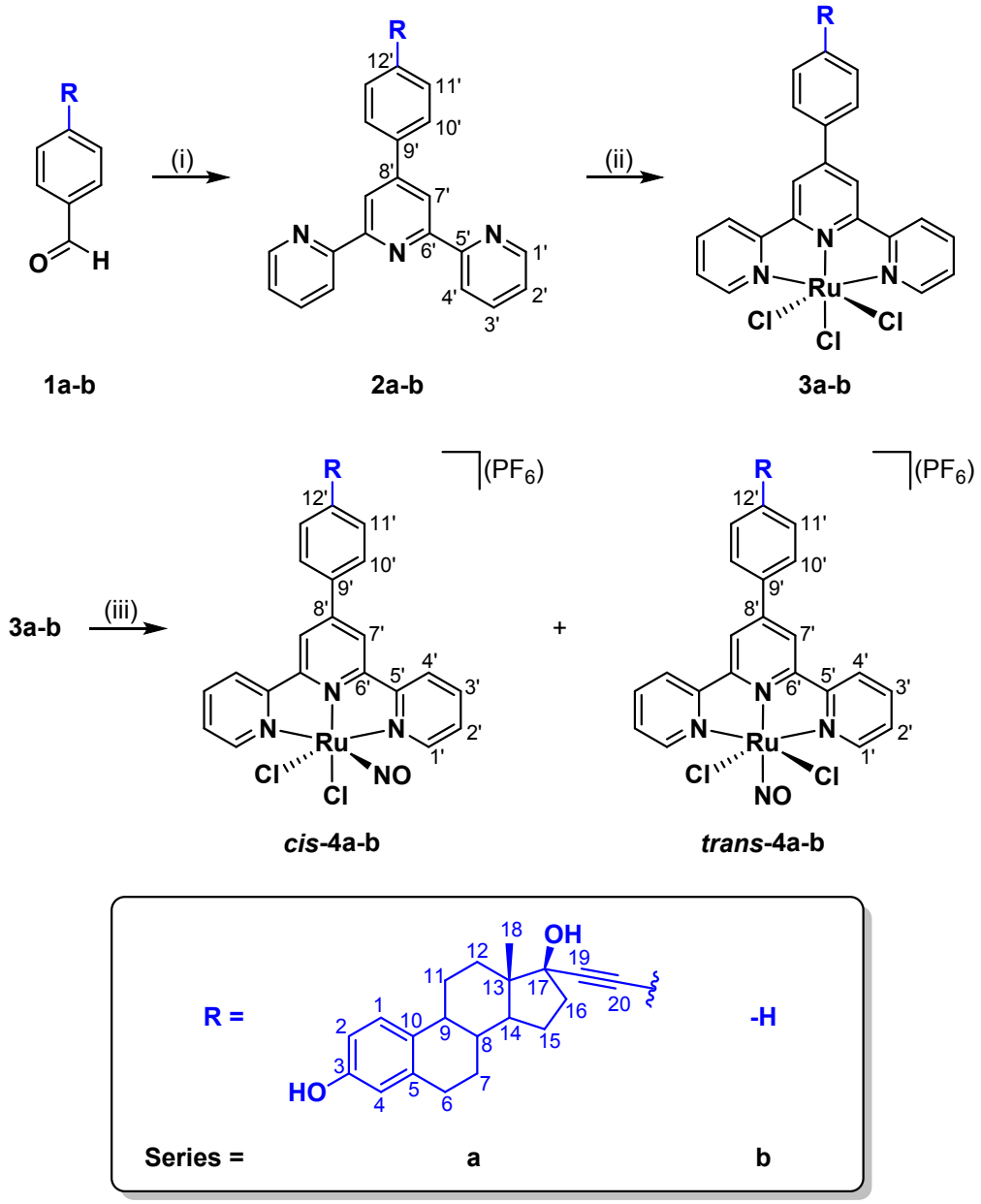

Scheme 1. Synthesis and numbering for ruthenium nitrosyl complexes ***cis*-4a-b** and ***trans*-4a-b**. Reagents and conditions: (i) 2-acetylpyridine, KOH, NH_4OH, MeOH, reflux; (ii) $RuCl_3xH_2O$, EtOH, reflux; (iii) $NO_{(g)}$, DMF, 85 °C, then HPLC purification and $NH_4PF_{6(aq)}$.

The identity and purity of the prepared ruthenium complexes and of the ligands and synthetic intermediates were verified employing a combination of spectroscopic techniques such as multinuclear $^1H/^{13}C$-NMR and IR spectroscopies, and MS/HRMS or elemental analysis. Although a complete unequivocal assignment of the NMR signals for the steroidal backbone is out of the scope of this paper, characteristic NMR signals were systematically assigned employing a combination of homonuclear ($^1H/^1H$) COSY/NOESY and heteronuclear ($^1H/^{13}C$) HSQC/HMBC 2D-NMR techniques. Additionally, as discussed in detail below (*vide infra*), the molecular structure of complex ***trans*-4a** was corroborated by single-crystal X-Ray diffraction (SXRD).

View Article Online
DOI: 10.1039/D3DT03480A

It seems important to clarify that taking into account the purpose of studying biological properties of these steroidal ruthenium nitrosyl complexes, we initially targeted their isolation and characterization as the water-stable *trans*(NO,OH)-[$Ru^{II}NO$(R-tpy)Cl_2](PF_6) species **Ph-tpy-RuNO** and **EE-Ph-tpy-RuNO**, which could be eventually prepared from the ***cis*-** and ***trans*-4a-b** complexes as previously described for **Ph-tpy-RuNO**.[37] Unfortunately, significant difficulties were found when attempting the isolation of **EE-Phtpy-RuNO**, precluding its isolation. Nevertheless, our group has previously demonstrated that a clean conversion to the desired complexes can be obtained within diluted solutions of the *cis*(Cl,Cl)- or *trans*(Cl,Cl)-[$Ru^{II}NO$(R-tpy)Cl_2](PF_6) in water after stirring for 72 hours.[37, 51] Therefore, and for consistency reasons, the two final water-stable ruthenium nitrosyls were not isolated, but studied *in situ* as obtained in these conditions.

Hydrolysis experiments and UV-visible spectroscopy

In this section we present a study of the hydrolysis of complexes ***trans*-4a-b** into their corresponding *trans*(NO,OH)-[Ru^{II}(NO)(R-tpy)(OH)(Cl)](PF_6) species (**EE-Phtpy-RuNO** and **Phtpy-RuNO**) and a discussion of the optical absorption properties of all the investigated RuNO complexes supported by TD-DFT computations. As previously discussed, the latter compounds are the two main molecular targets for the present study, following previous investigations from our group showing that this type of RuNO complexes are stable in water, where they retain excellent NO˙ releasing capabilities.[36-37] Although their isolation can result significantly challenging (*vide supra*), these complexes can otherwise be conveniently studied *in situ* as prepared from stirring dilute aqueous solutions of pure samples of their dichlorido-RuNO counterparts.[36]

The hydrolysis for the current set of RuNO complexes is illustrated in Figure 1a, showing the transformation in water of pure ***trans*-4a** and ***trans*-4b** into **EE-Phtpy-RuNO** and **Phtpy-RuNO**, respectively. As depicted in Figures 1b-c, the reactions were monitored by recording the changes in the electronic absorption profile of the complexes in water (with 0.5 % DMSO) for 72 hours. In these conditions, these complexes exhibited a significant blue shift of their lowest energy band located at λ = 382 and 350 nm for **EE-Phtpy-RuNO** and **Phtpy-RuNO**, respectively, in good agreement with our previous observations on structurally related complexes.[36-37] An additional important clarification is that water with a pH = XX was used for the hydrolyses; here that these procedures led to relatively constant absorption profiles, indicating the end of the reaction. Moreover, the completeness and nature of these reactions were corroborated by MS analyses at the beginning and at the end of the reaction, satisfactorily showing the dominant presence of the targeted products at the end of these

View Article Online
DOI: 10.1039/D3DT03480A

hydrolyses, as exemplified for ***trans*-4a** in the Supporting Information (Figure S5). Importantly, these results demonstrate that asides from the Cl→OH ligand exchange, these complexes remained stable in these conditions, without nucleophilic attacks by water that could potentially transform the nitrosyl into a nitrite, leading to complexes of impeded NO· release capabilities as discussed in detail elsewhere.[34,37]

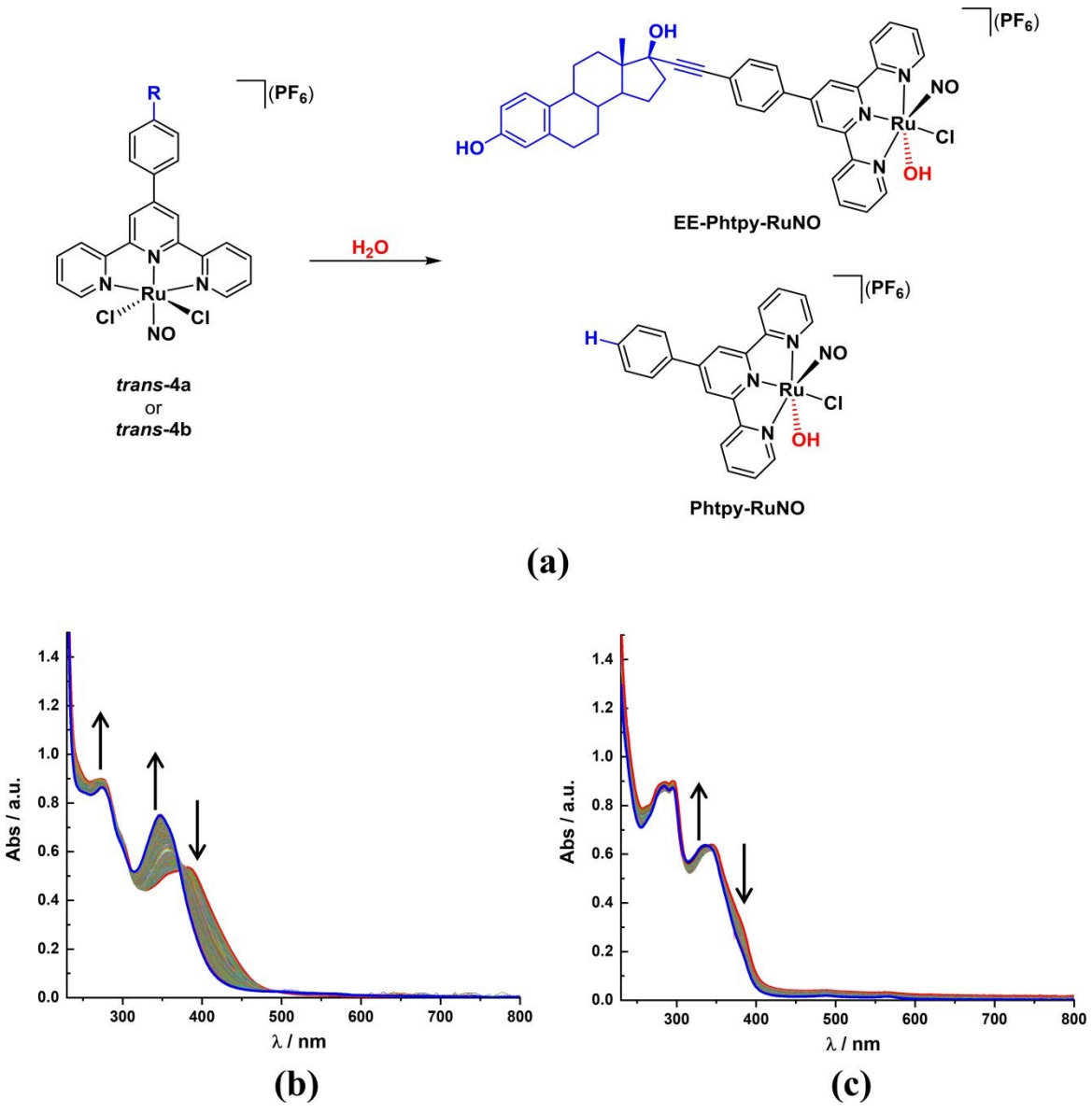

Figure 1. (a) Schematic representation of the hydrolysis of ***trans*-4a** and ***trans*-4b** towards **EE-Phtpy-RuNO** and **Phtpy-RuNO**, respectively; (b) Spectral evolution observed for the hydrolysis (5.0×10^{-5} M in water + 0.5 % DMSO) during 72h at 25 °C and pH = 6.4 for (b) ***trans*-4a** and (c) ***trans*-4b**.

View Article Online
DOI: 10.1039/D3DT03480A

Having addressed the preparation of complexes **EE-Phtpy-RuNO** and **Phtpy-RuNO**, we will now discuss their electronic absorption profiles and those of the dichlorido analogues. The analysis is supported by TD-DFT computations at the CAM-B3LYP/6-31G* level of theory from fully optimized geometries of these complexes. Experimental and computed data are gathered in Table 1 and in Supplementary Figures S1-S2, depicting a satisfactory agreement with a slight blue-shift for the lowest energy band, paralleling previous reports on structurally related complexes.[36-37, 48] It should be noted that although ***cis***- and ***trans***-**4b** have already been discussed elsewhere,[48] these complexes are discussed here as they allow assessing the effects of the biological recognition fragment (**EE**) on the optical properties.

Table 1. Experimental and TD-DFT computed (CAM-B3LYP/6-31*) optical absorption data for complexes ***cis*-4a-b** and ***trans*-4a-b** (in acetonitrile) and complexes **EE-Phtpy-RuNO** and **Phtpy-RuNO** (in water).

Compound	**UV-Vis** λmax [nm] (ε[molL^{-1}cm^{-1}])	**TD-DFT** λmax [nm] (*f*)	transition	CI expansion	dominant character
***cis*-4a**	352 (19300)	329 (0.938)	1 → 8	59% $\chi_{191\rightarrow193}$	CC-Ph → RuNO
	274 (25500)	282 (0.101)	1 → 17	16% $\chi_{188\rightarrow195}$ + 14% $\chi_{191\rightarrow195}$ + 13% $\chi_{182\rightarrow193}$	CC-Ph-tpyCl → tpyRuNO
		282 (0.139)	1 → 18	21% $\chi_{191\rightarrow195}$ + 11% $\chi_{182\rightarrow193}$ + 10% $\chi_{188\rightarrow195}$	CC-Ph-tpyCl → tpyRuNO
		263 (0.127)	1 → 29	26% $\chi_{186\rightarrow196}$ + 19% $\chi_{185\rightarrow195}$	tpyCl → tpyRuNO
***cis*-4b**[a]	330 (17400)	299 (1.528)	1 → 12	60% $\chi_{113\rightarrow114}$	Ph → RuNO
	284 (24600)	262 (0.183)	1 → 24	32% $\chi_{111\rightarrow117}$ + 19% $\chi_{106\rightarrow114}$	tpy → tpyRuNO
		247 (0.200)	1 → 32	48% $\chi_{106\rightarrow114}$ + 28% $\chi_{111\rightarrow117}$	tpyCl → RuNO
***trans*-4a**	382 (16500)	341 (0.814)	1 → 8	73% $\chi_{191\rightarrow193}$	CC-Ph → RuNO
	359 (18000)	327 (0.159)	1 → 9	39% $\chi_{188\rightarrow193}$ + 32% $\chi_{187\rightarrow193}$	Ph-tpyRuCl$_2$ → RuNO
	274 (28000)	265 (0.136)	1 → 28	38% $\chi_{191\rightarrow195}$ + 19% $\chi_{191\rightarrow193}$	CC-Ph → tpyRuNO
		263 (0.235)	1 → 29	35% $\chi_{188\rightarrow196}$ + 16% $\chi_{185\rightarrow195}$	tpyRuCl$_2$ → tpyRuNO
		261 (0.157)	1 → 31	42% $\chi_{187\rightarrow195}$ + 21% $\chi_{188\rightarrow195}$	CC-Ph-tpyRuCl$_2$ → tpyRuNO
***trans*-4b**[a]	350 (18800)	326 (0.162)	1 → 8	39% $\chi_{110\rightarrow114}$ + 26% $\chi_{111\rightarrow114}$	Ph-tpyRuCl$_2$ → RuNO
		311 (0.363)	1 → 10	71% $\chi_{113\rightarrow114}$	Ph → RuNO
	298 (23100)	277 (0.216)	1 → 21	25% $\chi_{107\rightarrow114}$ + 17% $\chi_{108\rightarrow115}$ + 14% $\chi_{102\rightarrow115}$ + 13% $\chi_{113\rightarrow116}$	tpyCl$_2$ → RuNO
	289 (22000)	262 (0.156)	1 → 26	24% $\chi_{111\rightarrow117}$ + 20% $\chi_{105\rightarrow114}$ + 13% $\chi_{112\rightarrow113}$ + 13% $\chi_{109\rightarrow116}$	Ph-tpyRuCl$_2$ → tpyRuNO

View Article Online
DOI: 10.1039/D3DT03480A

	270 (23500)	245 (0.201)	$1 \rightarrow 35$	33% $\chi_{110\rightarrow117}$ + 25% $\chi_{107\rightarrow114}$	Ph-tpyRuCl$_2$ → tpyRuNO
EE-Phtpy-RuNO[b]	347 (18800)	319 (1.109)	$1 \rightarrow 8$	67% $\chi_{187\rightarrow189}$	CC-Ph → tpyRuNO
	273 (21600)	272 (0.170)	$1 \rightarrow 15$	63% $\chi_{183\rightarrow190}$	tpy → RuNO
		250 (0.159)	$1 \rightarrow 29$	16% $\chi_{173\rightarrow190}$ + 15% $\chi_{167\rightarrow190}$ + 10% $\chi_{183\rightarrow192}$ + 8% $\chi_{174\rightarrow189}$	tpyCl$_2$ →RuNO
		234 (0.148)	$1 \rightarrow 39$	22% $\chi_{175\rightarrow189}$ + 13% $\chi_{183\rightarrow192}$ + 11% $\chi_{176\rightarrow189}$ + 10% $\chi_{187\rightarrow193}$	CC-Ph-tpy → tpyRuNO
Phtpy-RuNO[b]	337 (14500)	291 (0.483)	$1 \rightarrow 10$	62% $\chi_{109\rightarrow110}$	Ph → RuNO
	284 (20100)	258 (0.140)	$1 \rightarrow 21$	37% $\chi_{106\rightarrow113}$ +15% $\chi_{103\rightarrow110}$ + 13% $\chi_{106\rightarrow111}$	Ph-tpy→RuNO

[a]- Experimental data from Ref 48. [b]- Experimental data presented as recorded from solutions of their ***trans*-4a-b** precursors stirred for 72 h in water (+ 0.5 % DMSO).

The optical absorption spectra for the investigated RuNO complexes are presented in Figure 2a, showing the ubiquitous presence of two main bands, located at λ = 330 – 382 nm and λ = 270 – 274 nm, with similar extinction coefficients (ε). In spite of their different coordination spheres, the origin of these electronic transitions is similar along the whole series. Indeed, the lower energy band involves in every case a single excitation from a molecular orbital (MO) located at the ethynyl-phenyl or phenyl substituents of the terpyridyl ligands towards the lowest-lying unoccupied MO (LUMO) of the complex (For details see the Supporting Information, Figure S2). Because the LUMO bears a strong antibonding character for the Ru-NO submolecular fragment, the electronic excitation among these orbitals accounts for NO$^{\cdot}$ release, in good agreement with the photoreactivity of these complexes under irradiation at these wavelengths (*vide infra*). Conversely, the higher energy bands correspond largely to π -π^* intraligand excitations, not associated with NO$^{\cdot}$ release, that will not be discussed in detail here.

The molecular orbital energy diagram presented in Figure 2b allows introducing further remarks on the electronical properties of this family of complexes. While as previously mentioned they share rather similar absorption profiles, some features deserve further clarification. First, regardless of the coordination sphere around the Ru^{II} metal center, a redshift of λ = 12 – 32 nm for the lowest energy band was systematically observed in the case of RuNO complexes bearing the **EE** recognition fragment (***cis*-4a**, ***trans*-4a** and **EE-Phtpy-RuNO**), when compared to their nonsteroidal counterparts (***cis*-4b**, ***trans*-4b** and **Phtpy-RuNO**). This effect is related to a reduction of the energy gap between the involved frontier orbitals, arising from a more extended electron delocalization in the steroidal derivatives due to the presence of an electron-rich nonterminal acetylene. It should be noted that

View Article Online
DOI: 10.1039/D3DT03480A

alkynes such as that present in **EE** have very poor electrondonating/withdrawing capabilities, reflected by their Hammet constants (*e.g.* $\sigma_p = 0.03$ for -C≡C-CH_3).[52] These functional groups should therefore play negligible roles as electron donors or acceptors in the present complexes, where they should indeed participate primarily by extending the electron delocalization.

The second observation is the fact that complexes having an anionic (chlorido/hydroxido) ligand *trans* to the coordinated nitrosyl appeared blueshifted in comparison with their analogues having the nitrosyl in an equatorial position (***trans*-4a-b**). This effect has been observed for several other structurally-related RuNO complexes[48, 53] but no explanation has been provided so far. Comparing the localization of the involved MOs for a given pair of complexes computed in the same solvent, *e.g.* ***cis*-4a** and ***trans*-4a**, does not provide an explanation, as these MOs are localized in a virtually identical manner. However, the energy of the LUMO for complexes with an anionic ligand *trans* to the nitrosyl is significantly higher, indicating a weaker electron withdrawing effect played by the coordinated nitrosyl ligand. For example, the LUMO of ***cis*-4a** is about 0.16 eV higher in energy than that of ***trans*-4a**. While a further direct comparison of these two complexes with **EE-Phtpy-RuNO** is not possible as the latter is not studied in the same solvent, it nevertheless shares an anionic ligand *trans* to the nitrosyl, and thus a similar origin is expected for its blueshifted absorption. This explanation is supported by the structural analysis presented below (*vide infra*) that indicates the presence of a coordinated nitrosyl ligand with reduced electron withdrawing capabilities for complexes bearing an anionic ligand *trans* to the nitrosyl.

View Article Online
DOI: 10.1039/D3DT03480A

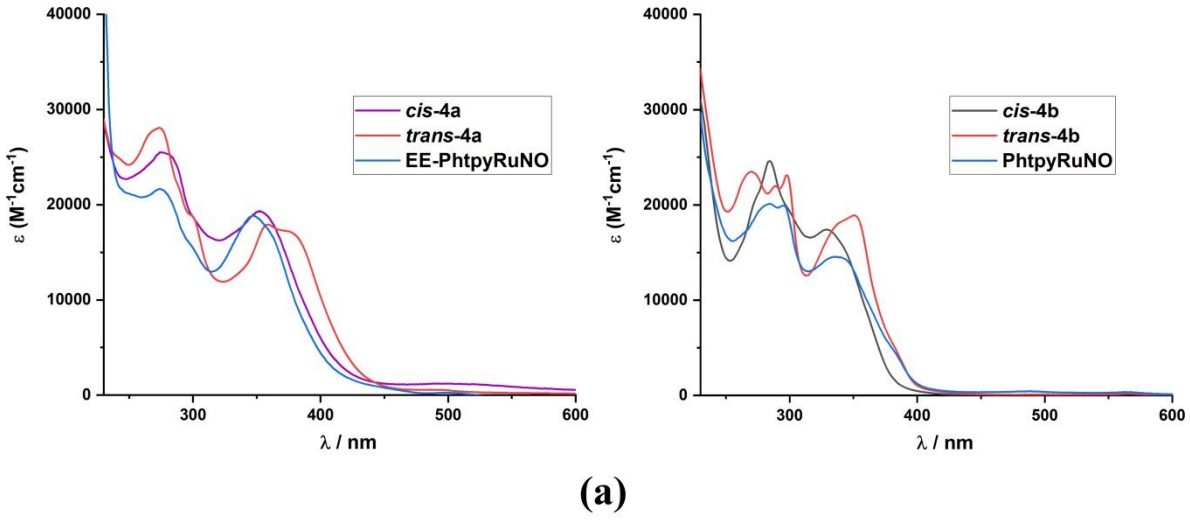

(a)

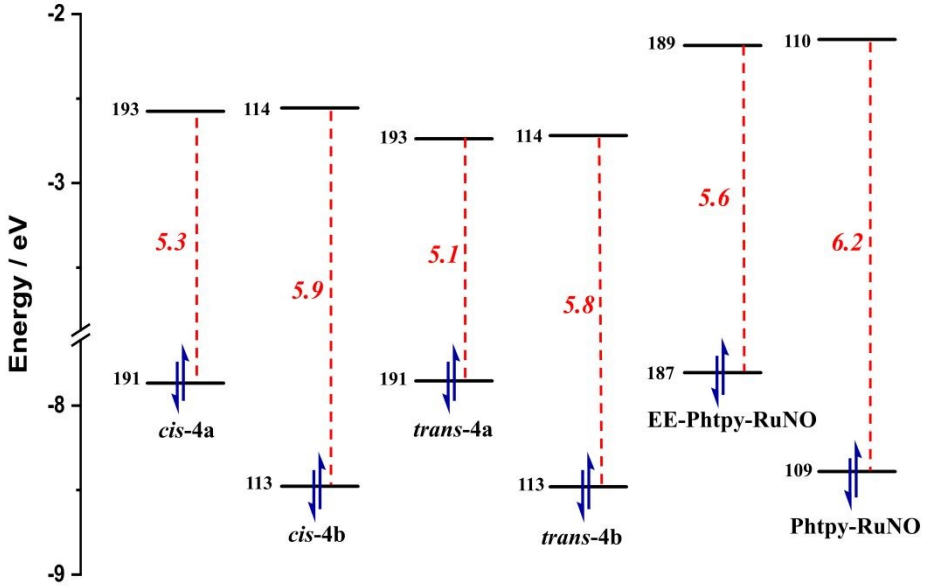

(b)

Figure 2. (a) UV-visible absorption spectra for steroidal ruthenium nitrosyl complexes (10^{-5} M, 25 ˚C). Spectra for complexes ***cis*-4a-b** and ***trans*-4a-b** were recorded in acetonitrile, while those of **EE-Phtpy-RuNO** and **Phtpy-RuNO** were registered from solutions of their ***trans*-4a-b** precursors after stirring for 72 h in water (+ 0.5 % DMSO). (b) TD-DFT computed energy diagram for relevant molecular orbitals involved in the lowest energy absorption bands related to NO release at the CAM-B3LYP/6-31G* level of theory with energy differences between the involved orbitals in red. Molecular orbital representations are included as Supporting Information (Figure S2).

View Article Online
DOI: 10.1039/D3DT03480A

Structural Characterization

After discussing the electronic properties of the RuNO complexes, we will now present a structural analysis aimed at characterizing the Ru-NO bonding in these complexes. As changes in bond order manifest as a shift of the corresponding vibrational frequency, IR spectroscopy represents a valuable tool to investigate the bond strength between Ru and the coordinated nitrosyl. In the study of ruthenium nitrosyls, IR spectroscopy is used primarily for analyzing the charge of the coordinated NO ($NO^+/NO^-/NO^{\cdot}$); the stretch of the nitrosyl indeed gives rise to absorption bands appearing at clearly distinct spectral intervals.[54-55] More subtle changes can also be studied to unveil slight deviations from one of the coordination modes of this non-innocent ligand.

The νNO stretch vibrations for these complexes are presented in Table 2 as measured in the solid state by FT-IR (ATR) spectroscopy. The experimental results were compared to their scaled[56] analytical frequencies computed by DFT on the isolated molecules to discard variations experimentally arising from solid-state effects. Experimentally appearing in the range of ν = 1834 – 1911 cm^{-1}, the observed νNO frequencies are in good agreement with the Ru^{II}-NO^+ configuration expected for this class of metal nitrosyls, corresponding to a $\{Ru\text{-}NO\}^6$ electronic configuration in the Enemark-Feltham notation,[57] indicating a total of 6 p/d electrons being shared between the metal and the nitrosyl. While an alternative Ru^{III}-$NO^{\cdot}$ configuration could be also envisioned, such possibility is disregarded considering the observed νNO stretch frequencies and the diamagnetic nature of these complexes.

Table 2. Experimental (FT-IR/ATR) and DFT-computed (B3PW91/6-31G*, scaled[56]) νNO stretch frequencies for the investigated RuNO complexes.

	***cis*-4a**	***cis*-4b**[a]	***trans*-4a**	***trans*-4b**[a]	**EE-Phtpy-RuNO**	**Phtpy-RuNO**[b]
FT-IR	1897	1911, 1897	1899	1907	Not isolated	1834
DFT	1921	1921	1930	1929	1882	1881

[a]- Experimental data from Ref 48. [b]- Experimental data from Ref 37.

It should be noted that the experimental νNO stretch frequencies show lower values for complexes bearing an anionic ligand *trans* to the nitrosyl, for example when comparing ***cis*-4b** and **Ph-tpyRuNO** vs ***trans*-4b**, with the trend being clearly consistent along the whole series for the computed DFT frequencies. This difference is attributed to an enhanced Ru-NO π-backbonding in complexes bearing anionic ligands, *trans* to the nitrosyl. Indeed, as this process populates π* orbitals in the nitrosyl, it reduces the N-O bond order, lowering its charge and electron withdrawing capabilities and shifting the stretch frequency to lower values. In fact, the enhanced Ru-NO π-backbonding has the dual effect of strengthening and weakening the Ru-N and N-O bonds,

View Article Online
DOI: 10.1039/D3DT03480A

respectively, which normally alters the geometry for the coordinated nitrosyl. To verify this, bond distances and angles for the Ru-NO submolecular fragment in the DFT-optimized geometries of these complexes were inspected. The average values, presented in Figure 3, indeed depict lower Ru-N-O angles, as well as shorter Ru-N and longer N-O bond distances for complexes featuring an anionic monodentate ligand *trans* to the nitrosyl, thus supporting the enhanced Ru-NO π-backbonding and a reduced withdrawing capability for the coordinated nitrosyl in these complexes.

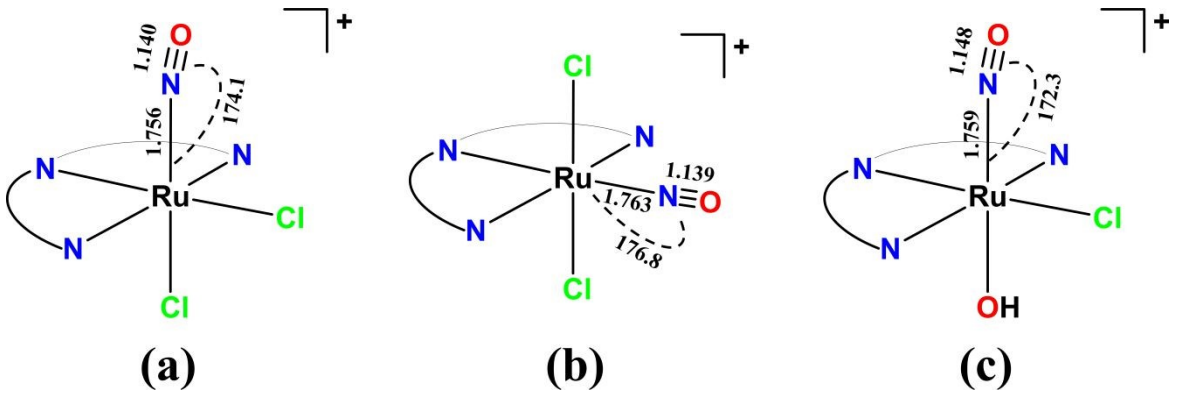

Figure 3. Selected average bond lengths [Å] and angles [°] computed at the B3PW91/6-31G* level for ***cis*-4a-b** (a), ***trans*-4-a-b** (b) and **EE-Phtpy-RuNO/Phtpy-RuNO** (c).

It should be noted that significant experimental evidence for the geometrical differences introduced by an anionic ligand *trans* to the nitrosyl, and discussed above for the DFT-optimized geometries, can be found in literature. For instance, single-crystal X-Ray diffraction (SXRD) experiments for ***cis*-4b** and ***trans*-4b** do show a clearly reduced Ru-N-O angle for the former, as well as for other structurally related complexes.[48] To further explore these geometrical differences, in this contribution we attempted the crystallization of the investigated steroidal complexes. Nevertheless, crystals of enough quality for SXRD determinations could be obtained only for ***trans*-4a**, precluding further experimental comparisons. The crystal structure and crystallographic data are shown in Figure 4 and Supplementary Table S1, respectively. The complex crystallized as a diethyl ether/acetonitrile solvate in the monoclinic $P2_1$ chiral spacegroup, with 2 molecules of the complex per unit cell. The presence of a single and highly disordered PF_6 counterion per complex confirmed its expected +1 charge as well as its $\{Ru\text{-}NO\}^6$ configuration.

Regarding the geometry of the nitrosyl, the associated Ru-N/N-O bond distances and Ru-N-O angle correlated well with those discussed before for the DFT-optimized geometry of this type of complexes and were found similar to those of its non-steroidal analogue ***trans*-4b**.[48] On the other hand, the **EE** fragment showed the typical annular conformations for these tetracyclic fused steroidal cores,[58] without significant variations with respect to the crystal structure informed for this specific steroid.[59] Intriguingly, the molecular structure of ***trans*-4a** showed the 1,4-phenylene disordered over two crystallographically independent positions (in a 0.84/0.16 ratio), as a feature that could be

View Article Online
DOI: 10.1039/D3DT03480A

associated with rotational motion in the solid state. Although no further experiments were conducted to investigate this interesting possibility, extensive evidence for the occurrence of such dynamic processes is reported for structurally-related steroidal derivatives.[60]

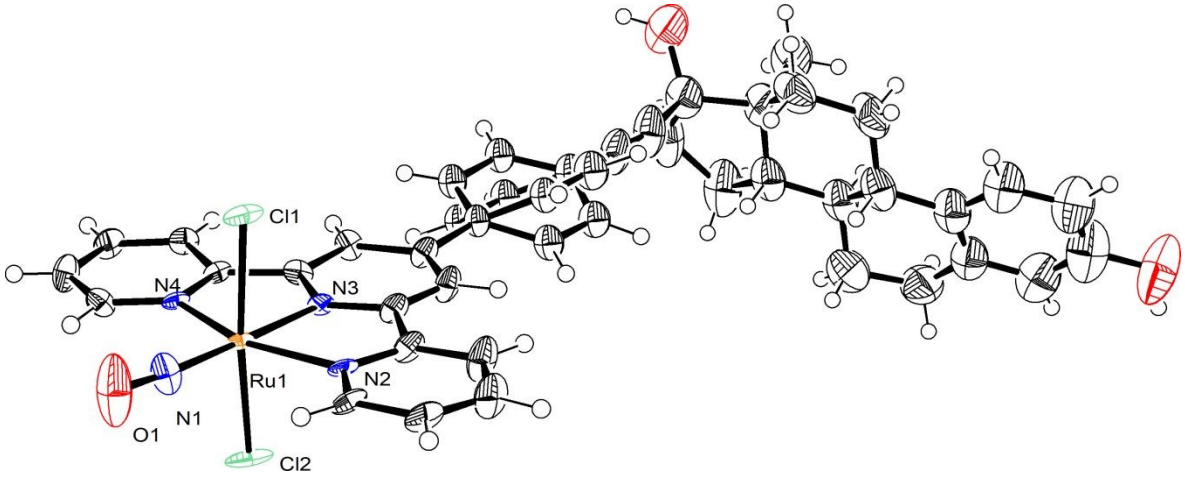

Figure 4. Asymmetric unit for complex ***trans*-4a**. A disordered PF_6 counterion and two solvent molecules (acetonitrile, diethyl ether) are omitted for clarity. Thermal ellipsoids are drawn at 50 % probability for every atom other than hydrogen. Selected bond lengths [Å] and angles [°]: Ru1-N1 1.755(3), N1-O1 1.130(4), Ru1-Cl1 2.336(2), Ru1-Cl2 2.331(2), Ru1-N2 2.084(2), Ru1-N3 2.003(2), Ru1-N4 2.079(2), Ru1-N1-O1 175.4(7), Cl1-Ru1-Cl2 173.0(1), N1-Ru1-N3 179.0(2), N2-Ru1-N4 156.8(1).

NO photorelease

The NO· release capabilities of the obtained RuNO complexes were investigated in solution under irradiation at λ = 365 nm, with the exception of ***cis*-4b** and ***trans*-4b** that were already investigated by our group under the same experimental conditions.[48] Considering the intended investigations in biological media, the photochemical properties for the target complexes **EE-Phtpy-RuNO** and **Phtpy-RuNO** were investigated in water (+0.5 % DMSO), as formed *in situ* from their corresponding dichlorido precursors (***trans*-4a-b**). Conversely, ***cis*-4a** and ***trans*-4a** were investigated in acetonitrile due to their aforementioned instability in aqueous media. Under irradiation at this wavelength, all these complexes are excited at their lowest energy absorption band, which should lead to NO· release according to our previous discussions on their electronic absorption spectra (*vide supra*).

The spectral evolution for the investigated complexes is shown in Figure 5, displaying rapid changes in absorbance at relatively low photon flux (I_0) values, as an early qualitative indication of the good photorelease efficiency of these complexes. HRMS measurements were carried out on the

View Article Online
DOI: 10.1039/D3DT03480A

photolyzed samples to gain an understanding on the nature of these photoreactions. The results, exemplified in the Supporting Information (Figure S6), showed the evolution of ***cis*-** and ***trans*-4a** towards the $[Ru^{III}Cl_2(\mathbf{EE\text{-}Phtpy\text{-}RuNO})(MeCN)]^+$ solvate, in good agreement with previous reports on related dichlorido-RuNO complexes.[48, 53] We were unfortunately unable to obtain analogous information on the corresponding photoproducts for **EE-Phtpy-RuNO** and **Phtpy-RuNO**, likely due to instability of the expected aqua solvate in the conditions of the HRMS measurements. Nonetheless, considering the similar spectral evolution for all the complexes with apparent isosbestic points located around λ = 350 and λ = 400 nm, a clean conversion to the corresponding aqua solvate for **EE-Phtpy-RuNO** and **Phtpy-RuNO** seems a reasonable assumption. Fitting of the time-dependent absorbance changes at two wavelengths to a photokinetic model considering an A → B reaction, resulted in relatively good fittings with average correlation coefficients in the R^2 = 0.97819 – 0.99958 interval.

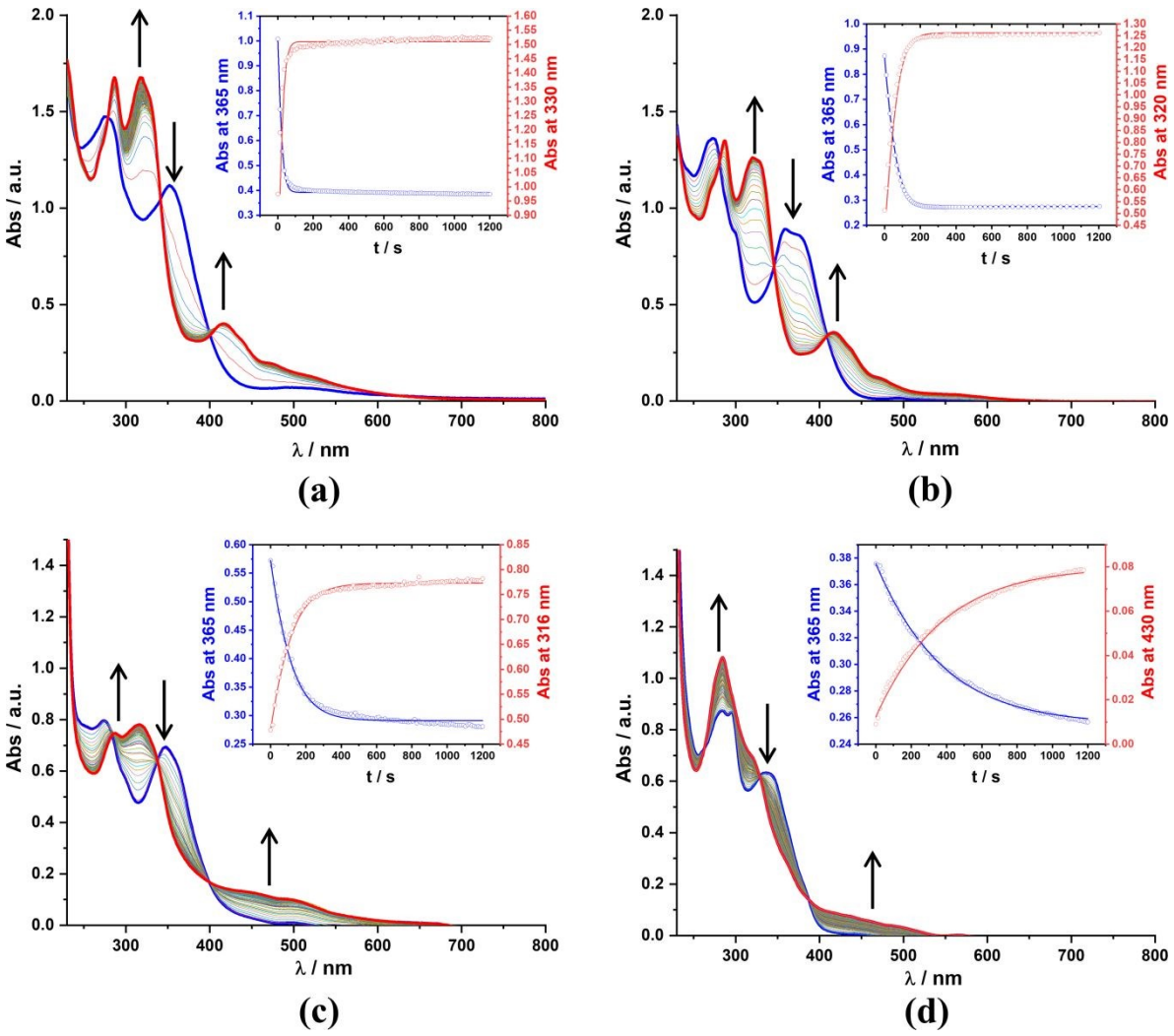

Figure 5. Spectral evolution under irradiation at λ = 365 nm for (a) ***cis*-4a** (5.8×10^{-5} M in acetonitrile, $I_0 = 6.8\times10^{-6}$ molL^{-1}s^{-1}); (b) ***trans*-4a** (4.9×10^{-5} M in acetonitrile, $I_0 = 7.9\times10^{-6}$ molL^{-1}s^{-1}); (c) **EE-Phtpy-RuNO** (3.7×10^{-5} M in water + 0.5 % DMSO, $I_0 = 7.1\times10^{-6}$ molL^{-1}s^{-1}) and (d) **Phtpy-RuNO** (4.38×10^{-5} M in water + 0.5 % DMSO, $I_0 = 6.18\times10^{-6}$ molL^{-1}s^{-1}). Insets show the time-dependent

View Article Online
DOI: 10.1039/D3DT03480A

changes in absorbance at two wavelengths and fitting of the experimental data to the data to the photokinetic model, with R^2 = 0.97819 – 0.99958.

The photochemical quantum yields of NO release (Φ_{NO}) for the investigated RuNO complexes, obtained taking into account the above considerations, are presented in Table 3. Although the Φ_{NO} values obtained for ***cis*-** and ***trans*-4a** and the previously informed[48] ***cis*-** and ***trans*-4b** are very high, such dichlorido-RuNO complexes are unstable in water, and thus cannot be straightforwardly considered for biological applications. On the other hand, the Φ_{NO} values for water-stable **EE-Phtpy-RuNO** and **Phtpy-RuNO**, although more modest, are still significant and may lead to biologically relevant NO concentrations, considering previous reports by our research group on structurally related RuNO complexes.[36-37]

Table 3. Photochemical quantum yields of NO release (Φ_{NO}) under irradiation at λ = 365 nm.

	Solvent	Φ_{NO}
***cis*-4a**	Acetonitrile	0.37
***cis*-4b**		0.39[a]
***trans*-4a**		0.10
***trans*-4b**		0.12[a]
EE-Phtpy-RuNO	Water (+0.5 % DMSO)	0.06
Phtpy-RuNO		0.03

[a]- Data from Ref 48.

In any case, the efficient photorelease of NO· from the current family of RuNO complexes was systematically demonstrated employing two techniques. The first technique is the Griess test, which allows an indirect detection of NO· as oxidized to nitrites.[61] This is exemplified in Figure 6a for **EE-Phtpy-RuNO** in aqueous solution, where photogenerated nitrites react *in situ* with the Griess reagent to give rise to a colored azo dye, which absorbs strongly around λ = 530 nm, thus constituting an indirect demonstration of NO· release. Direct demonstrations of NO· release were also achieved using continuous-wave EPR. As exemplified in Figure 6b for ***trans*-4a** in acetonitrile, solutions of the complexes were mixed with equimolar amounts of the NO-selective [$Fe^{II}(MGD)_2$] spin trap, and the solution was irradiated continuously at λ = 365 nm for 10 minutes, giving rise to an increasing triplet signal with a *g*-factor of 2.028 and a hyperfine coupling constant, a_N = 1.19x10^{-3} cm^{-1}, which corresponds to a nitric oxide radical.[62]

View Article Online
DOI: 10.1039/D3DT03480A

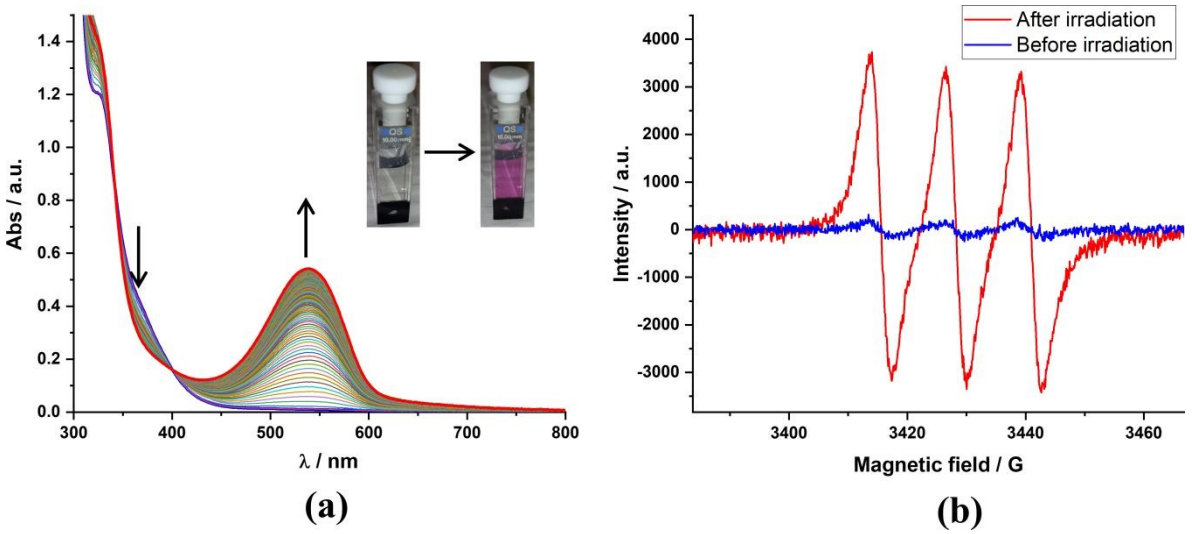

Figure 6. Representative experiments demonstrating nitric oxide release triggered by irradiation at λ = 365 nm, as evidenced by (a) the spectral evolution in water (+ 0.5 % DMSO) for **EE-Phtpy-RuNO** in the presence of the Griess reagent leading to the formation of a pink azo dye[61] (inset: color change before and at the end of the photoreaction) and (b) the observation of a triplet EPR signal in presence of the NO-selective $[Fe^{II}(MGD)_2]$ spin trap[62] for ***trans*-4a** in acetonitrile.

LogP Measurements and Biological Tests

As mentioned in the introduction, physicochemical properties of drugs play a decisive role in cell penetration.[6] For example, being a highly lipophilic moiety, a steroid such as **EE** may significantly increase the lipophilicity of the complex, favoring passive diffusion across the plasma membrane. To explore this possibility, we measured the *n*-octanol/water partition coefficient (logP) for **Phtpy-RuNO** and **EE-Phtpy-RuNO**. The measurements were performed spectroscopically as reported elsewhere[64] and calculated following Equation 1, where Abs_{Oct}^{275} and $Abs_{H_2O}^{275}$ are the absorbances of the complexes at λ = 275 nm in *n*-octanol and water, respectively (for details see the Supporting Information, Figures S7-S8).

$$logP = \log\left(\frac{Abs_{Oct}^{275}}{Abs_{H_2O}^{275}}\right) \quad (1)$$

The logP values thus obtained were of -1.215 ± 0.243 (**Phtpy-RuNO**) and 0.336 ± 0.063 (**EE-Phtpy-RuNO**), indicating a drastic increase in lipophilicity for **EE-Phtpy-RuNO** caused by the attachment of **EE**. Consequently, **EE-Phtpy-RuNO** is expected to interact more favorably with the lipids in the cell membrane, favoring its uptake.

In order to determine whether **EE** promotes cell penetration, we chose to carry out biological experiments with human dermal fibroblasts which have indeed been shown to express mRNA for androgen receptors and estrogen receptors (ERα and ERβ).[63] We thus chose to work with this cell type to determine by ICP-MS the penetration of Ru element within cells after 3h of incubation at

View Article Online
DOI: 10.1039/D3DT03480A

37°C. For that purpose, cells were exposed to 10.1µg of Ru within either **Phtpy-RuNO** or **EE-Phtpy-RuNO** complexes. Ru quantification revealed a weak rate of penetration of 0.04% and 0.42% respectively for **Phtpy-RuNO** or **EE-Phtpy-RuNO** (Figure 7). Although this rate appears very low, it is interesting to note that the presence of **EE** favored the penetration of the **EE-Phtpy-RuNO** complex, since 9.75 times more of Ru penetrated in the cells than in the condition without the **EE** recognition fragment, i.e., the **Phtpy-RuNO** complex.

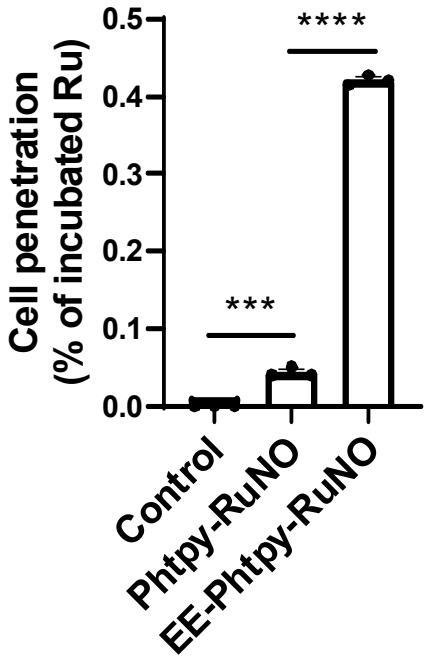

Figure 7. Intracellular Ru quantification by ICP-MS. Human dermal fibroblasts were incubated for 3h at 37°C with 10.1 µg of Ru within either **Phtpy-RuNO** or **EE-Phtpy-RuNO** complexes, and then Ru was quantified by ICP-MS. n=3. Individual biological replicates are represented ± SEM, and analyzed by 1-way ANOVA followed by Tukey's multiple comparisons test.

While the results above gratifyingly indicate that the introduction of **EE** enhances significantly the entrance of the target RuNO complex, further mechanistic studies are necessary to confirm that the enhanced uptake of **EE-Phtpy-RuNO** is mediated by an interaction of the **EE** fragment with the ER receptors.

CONCLUSION

In this manuscript we explored the attachment of 17α-ethinylestradiol (**EE**), a well-known steroidal hormone, to a ruthenium nitrosyl (RuNO) complex as a drug delivery strategy aimed at enhancing the cell uptake of these photoactive nitric oxide (NO·) donors. With the possibility of delivering NO· locally in a highly controlled manner, some of these complexes have already become appealing candidates for applications in photoactivated chemotherapy. Nonetheless, being charged, highly polar

View Article Online
DOI: 10.1039/D3DT03480A

and relatively large molecules, the cell uptake efficiency of most RuNO complexes seems intuitively compromised. The attachment of **EE** was therefore aimed to work as a molecular Trojan horse in the sense that a favorable interaction of the attached **EE** with the estrogen receptors (ER) would favor the cell uptake of the RuNO complex by ER (over)expressing cells.

Our investigation was centered on systematically comparing two RuNO complexes, the steroidal derivative **EE-Phtpy-RuNO** and its reference complex lacking **EE** (**Phtpy-RuNO**). While the photophysical and photochemical properties remained relatively unchanged, an outstanding 10-fold enhancement of the cell uptake into human dermal fibroblasts was observed for **EE-Phtpy-RuNO**, gratifyingly demonstrating the significance of adding this biological recognition fragment. Additional studies are still needed to fully disclose if the significant uptake enhancement observed is indeed related to an active uptake mechanism involving an early interaction of the **EE** fragment with the ER, or if alternative mechanisms take place, such as an enhanced passive diffusion caused by the drastically different lipophilicities of these complexes. A detailed description of these processes may pave the way for the interesting possibility of delivering photoactive RuNO complexes into tissues overexpressing the ER, such as the most common types of breast cancer.

EXPERIMENTAL SECTION

Materials and Equipment

All the starting materials were obtained from commercial sources (Merck, Alfa Aesar); the solvents were of analytical grade and used without further purification. Column chromatography was performed on silica gel (230-400 mesh) employing an appropriate eluent. Infrared spectra were recorded on a Perkin Elmer Spectrum 100 FT-IR spectrometer using a diamond ATR. MS and HRMS data were acquired using ThermoScientific LCQ Fleet and Agilent G1969A ESI-TOF spectrometers, respectively. Elemental analyses were performed at LCC using a Perkin Elmer 2400 series II Instrument. The UV-visible spectra were obtained on a Hewlett Packard 8454A spectrometer. Aldehyde **1a** and ligand **2b** and its ruthenium complexes **3b**, ***cis*-4b** and ***trans*-4b** were prepared following literature procedures[48-49] with minor modifications; spectral data were in good agreement.

NMR Spectroscopy

NMR spectra were recorded using Bruker Avance III 300/400 spectrometers at 298 K using deuterated solvents and standard pulse sequences; chemical shifts for ^{1}H- and ^{13}C-NMR data are relative to the residual nondeuterated solvent signal, fixed at $\delta = 7.26$ ($CDCl_3$) and 1.940 (CD_3CN) for ^{1}H-NMR and $\delta = 77.00$ ($CDCl_3$) and 1.320 (CD_3CN) ppm for ^{13}C-NMR. Chemical shifts are given in ppm with multiplicities abbreviated as singlet (s), doublet (d), doublet of doublets (dd), doublet of doublets of doublets (ddd), triplet of doublets (td) and multiplet (m).

X-Ray Diffraction Studies

View Article Online
DOI: 10.1039/D3DT03480A

Crystals of ***trans*-4a** were grown by slow diffusion of diethyl ether into a saturated solution of the complex in acetonitrile. Data were collected on a Bruker Kappa Apex II diffractometer equipped with a 30 W air-cooled microfocus source using MoKα radiation (λ = 0.71073 Å). An Oxford Cryosystems Cryostream cooling device was used to collect the data at low temperature (100(2) K). Phi and Omega scans were performed for data collection, an empirical absorption correction was applied and the structures were solved by intrinsic phasing method (ShelXT).[63] All non-hydrogen atoms were refined anisotropically by means of least-squares procedures on F^2 with CRYSTALS.[64] All the hydrogen atoms were refined isotropically at calculated positions using a riding model. The C16-C21 phenyl ring is disordered over two positions. The PF_6^- counterion is highly disordered; refinement of the model over three positions led to a satisfactory solution with 0.466, 0.377 and 0.157 occupancy ratios. Restraints were applied to regularize the geometries affected by disorders. The SQUEEZE[65] function of PLATON was used to remove the remaining electron density contribution of the highly disordered solvent molecules. Deposition Number 2299656 contains the supplementary crystallographic data for this paper. These data are provided free of charge by the joint Cambridge Crystallographic Data Centre and Fachinformationszentrum Karlsruhe Access Structures service.

Syntheses

4-[3,17β-dihydroxy-19-norpregna-1,3,5(10)-trien-20-yn-21-yl]benzaldehyde (**1a**). To a solution of ethinylestradiol (1.1026 g, 3.72 mmol), $Pd(PPh_3)_2Cl_2$ (0.1305 g, 0.186 mmol), CuI (0.0708 g, 0.372 mmol) and 4-bromobenzaldehyde (1.0324 g, 5.58 mmol) in THF (37 mL) was added triethylamine (1.53 mL) and the reaction was refluxed overnight under nitrogen. The reaction was allowed to chill to room temperature and concentrated *in vacuo*, the residue was redissolved in methylene chloride (100 mL), washed with NH_4Cl (aq, sat.) (3 x 40 mL), brine (1 x 40 mL) and water (1 x 40 mL) and evaporated to dryness. The crude product was purified by column chromatography using hexane/ethyl acetate 8/2 as eluent to yield 1.1264 g (2.81 mmol, 76 %) of **1a** as a beige solid. **^{1}H-NMR** δ (400 MHz, $CDCl_3$): 10.00 (s, 1H, H-25), 7.83 (d, J = 8.2 Hz, 2H, H-23), 7.59 (d, J = 8.2 Hz, 2H, H-22), 7.17 (d, J = 8.4 Hz, 1H, H-1), 6.64 (d, J = 11.2 Hz, 1H, H-2), 6.57 (d, J = 2.7 Hz, 1H, H-4), 2.87 – 2.79 (m, 2H), 2.51 – 2.31 (m, 3H), 2.28 – 2.06 (m, 3H), 2.00 – 1.70 (m, 7H), 1.58 – 1.35 (m, 5H), 0.95 (s, 3H, H-18). **^{13}C-NMR** δ ($CDCl_3$, 100 MHz): 191.45 (C-25), 153.35, 138.24, 135.48, 132.45, 132.19 (C-22), 129.53 (C-23), 129.26, 126.55 (C-1), 115.26 (C-4), 112.72 (C-2), 97.01, 85.27 (C-19), 80.47 (C-20), 49.98, 47.78, 43.66, 39.46, 39.09, 33.15, 29.61, 27.21, 26.45, 22.96, 12.88 (C-18). **HRMS** (ESI-TOF$^+$) *m/z*: $[M+H]^+$ Observed: 401.2111. Anal. calcd for $C_{27}H_{29}O_3$: 401.2117. Error: -1.50 ppm.

4'-(4-[3,17β-dihydroxy-19-norpregna-1,3,5(10)-trien-20-yn-21-yl]phenyl)-2,2':6',2''-terpyridine (**2a**, **EE-Phtpy**). To a solution of **1a** (2.765 g, 6.90 mmol) in methanol (50 mL) was added a mixture of 2-acetylpyridine (1.55 mL, 13.8 mmol), KOH (0.774 g, 13.8 mmol) and methanol (11 mL)

View Article Online
DOI: 10.1039/D3DT03480A

previously stirred at room temperature for 30 minutes. The reaction was stirred 2 hours at this temperature followed by addition of NH_4OH (18 mL, 30 %) and heating to reflux overnight. After adding additional NH_4OH (20 mL) and heating to reflux for 2 hours; a green oily material was formed, which was discarded. The aqueous phase was decanted and water was subsequently added to precipitate the product, which was collected, washed with water and cold ethanol to yield **2a** as a beige to light yellow solid (2.5244 g, 61 %). **^{1}H-NMR** δ (400 MHz, $CDCl_3$): 8.76 – 8.64 (m, 6H, H-1'/H-4'/H-7'), 7.94 – 7.86 (m, 2H, H-3'), 7.79 (d, *J* = 7.7 Hz, 2H, H-10'), 7.52 (d, *J* = 7.7 Hz, 2H, H-11'), 7.41 – 7.33 (m, 2H, H-2'), 7.13 (d, *J* = 8.4 Hz, 1H, H-1), 6.64 (d, *J* = 7.9 Hz, 1H, H-2), 6.57 (s, 1H, H-4), 2.88 – 2.72 (m, 2H), 2.55 – 1.70 (m, 13H), 1.60 – 1.31 (m, 5H), 0.94 (s, 3H, H-18). **^{13}C-NMR** δ ($CDCl_3$, 100 MHz): 155.99, 155.74, 153.74, 149.45, 148.94 (C-1'), 138.16, 137.93, 137.22 (C-3'), 132.27, 132.18 (C-11'), 127.16 (C-10'), 126.51 (C-1), 124.02 (C-2'), 123.71, 121.65 (C-4'), 118.83 (C-7'), 115.43 (C-4), 112.84 (C-2), 94.30, 85.68 (C-19), 80.41 (C-20), 49.84, 47.69, 43.60, 39.51, 39.14, 33.14, 29.67, 27.23, 26.49, 23.00, 12.93 (C-18). **HRMS** (ESI-TOF$^+$) *m/z* anal. calcd. for $C_{41}H_{38}N_3O_2$ $[M+H]^+$: 604.295854. Found: 604.2960. Error: 0.21 ppm.

[Ru^{III}(EE-Phtpy)Cl$_3$] (**3a**). A solution of **2a** (2.5244 g, 4.2 mmol) and $RuCl_3xH_2O$ (0.83 g) in ethanol (120 mL) was stirred under reflux for 7 hours. The mixture was concentrated in vacuo to ca. 50 mL and it was chilled to 0 ˚C. The dark red solid thus obtained was collected, washed with ethanol and ether. Then this crude product was purified by treatment with boiling ethanol (70 mL) followed by vacuum filtration and drying overnight. In this manner, 1.6575 g (2.04 mmol, 30 %) of **3a** were obtained as a black solid. **Elemental Analysis** found: C, 59.24; H, 5.15; N, 4.68. Required for $C_{41}H_{39}Cl_3N_3O_3Ru$; H_2O: C, 59.39; H, 4.74; N, 5.07.

*Preparation of complexes **cis-4a** and **trans-4a**.* Compound **3a** (382 mg, 0.47 mmol) was dissolved in dimethylformamide (8 mL) and the solution was bubbled with Ar for 15 minutes. After warming to 85 ˚C, gaseous nitric oxide, obtained by the dropwise addition of diluted HNO_3 on copper, was bubbled for 5 hours. After cooling to room temperature, the solution was concentrated *in vacuo* to a final volume of *ca.* 10 mL. A large excess of diethyl ether precipitated 377.5 mg of a brown powder 0.45 mmol, 95 %). This crude product was not soluble enough to be characterized by ^{1}H-NMR, but according to IR (ν_{NO} = 1875 cm^{-1}) and MS (*m*/*z* = 805.00), it was mainly constituted by a mixture of two species, the *cis*(Cl,Cl)- and *trans*(Cl,Cl)-[Ru^{II}(**EE-Phtpy**)(NO)Cl_2](Cl) complexes and a minor amount of the homoleptic complex [Ru^{II}(**EE-Phtpy**)$_2$](Cl)$_2$ (*m*/*z* = 654.33). Analytical samples of ***cis-***

View Article Online
DOI: 10.1039/D3DT03480A

and ***trans*-4a** and $[Ru^{II}(\mathbf{EE\text{-}Phtpy})_2](PF_6)_2$ were isolated from the crude product by HPLC ($MeOH/H_2O$ + 0.1% TFA) followed by metathesis with aqueous NH_4PF_6.

cis(Cl,Cl)-[Ru^{II}(EE-Phtpy)(NO)Cl$_2$](PF$_6$) (***cis*-4a**). Obtained as a brown solid. **^{1}H-NMR** δ (400 MHz, CD_3CN): 9.20 (dd, *J* = 6.1, 1.5 Hz, 2H, H-1'), 8.81 (s, 2H, H-7'), 8.73 (d, *J* = 7.5 Hz, 2H, H-4'), 8.49 (td, *J* = 7.9, 1.5 Hz, 2H, H-3'), 8.08 (d, *J* = 8.5 Hz, 2H, H-10'), 7.98 (ddd, *J* = 7.9, 5.5, 1.4 Hz, 2H, H-2'), 7.76 (d, *J* = 8.5 Hz, 2H, H-11'), 7.14 (d, *J* = 8.4 Hz, 1H, H-1), 6.60 – 6.54 (m, 2H, H-2/3-OH), 6.51 (d, *J* = 2.6 Hz, 1H, H-4), 3.48 (s, 1H, 17-OH), 2.84 – 2.77 (m, 2H), 2.44 – 2.31 (m, 3H), 2.28 – 2.19 (m, 2H), 1.54 – 1.32 (m, 6H), 0.93 (s, 3H, H-18). **HRMS** (ESI-TOF$^+$) *m/z* anal. calcd. for $C_{41}H_{37}Cl_2N_4O_3Ru$ [*M*-PF_6]$^+$: 805.1292. Found: 805.1281. Error: -1.37 ppm. **FT-IR** (ATR, cm^{-1}): 1897 (νNO). **UV-vis** (in acetonitrile) λ_{max} in nm (ε in $M^{-1}cm^{-1}$): 352 (19300), 274 (25500).

trans(Cl,Cl)-[Ru^{II}(EE-Phtpy)(NO)Cl$_2$](PF$_6$) (***trans*-4a**). Obtained as a pale brown/yellow solid. **^{1}H-NMR** δ (400 MHz, CD_3CN): 8.77 (ddd, *J* = 5.6, 1.5, 0.7 Hz, 2H, H-1'), 8.72 (s, 2H, H-7'), 8.67 (ddd, *J* = 8.1, 1.5, 0.7 Hz, 2H, H-4'), 8.40 (td, *J* = 7.9, 1.5 Hz, 2H, H-3'), 8.05 (d, *J* = 8.6 Hz, 2H, H-10'), 7.88 (ddd, *J* = 7.9, 5.6, 1.4 Hz, 2H, H-2'), 7.74 (d, *J* = 8.7 Hz, 2H, H-11'), 7.14 (d, *J* = 8.4 Hz, 1H, H-1), 6.60 – 6.53 (m, 2H, 3-OH/H-2), 6.51 (d, *J* = 2.7 Hz, 1H, H-4), 3.47 (s, 1H, 17-OH), 2.84 – 2.76 (m, 2H), 2.45 – 2.30 (m, 3H), 1.55 – 1.28 (m, 6H), 0.92 (s, 3H, H-18). **^{13}C-NMR** δ (CD_3CN, 100 MHz): 156.48, 155.94, 155.56, 155.16 (C-1'), 154.19, 143.49 (C-3'), 139.05, 135.26, 133.40 (C-11'), 132.61, 131.12 (C-10'), 129.50 (C-2'), 128.14, 127.71 (C-4'), 127.42, 123.73 (C-7'), 116.03 (C-4), 113.63 (C-2), 98.77, 85.04 (C-19), 80.79 (C-20), 50.88, 48.72, 44.63, 40.56, 39.90, 34.16, 30.31, 28.14, 27.46, 23.68, 13.85 (C-18). **HRMS** (ESI-TOF$^+$) *m/z* anal. calcd. for $C_{41}H_{37}Cl_2N_4O_3Ru$ [*M*-PF_6]$^+$: 805.1292. Found: 805.1285. Error: -0.87 ppm. **FT-IR** (ATR, cm^{-1}): 1899 (νNO). **UV-vis** (in acetonitrile) λ_{max} in nm (ε in $M^{-1}cm^{-1}$): 382 (16500), 359 (18000), 274 (28000)

[Ru^{II}(EE-Phtpy)$_2$](PF$_6$)$_2$. Obtained as a red solid. **^{1}H-NMR** δ (400 MHz, CD_3CN): 8.99 (s, 4H, H-7'), 8.64 (d, *J* = 8.0 Hz, 4H, H-4'), 8.20 (d, *J* = 8.5 Hz, 4H, H-10'), 7.94 (td, *J* = 7.8, 1.5 Hz, 4H, H-3'), 7.80 (d, *J* = 8.5 Hz, 4H, H-11'), 7.42 (dd, *J* = 5.6, 0.8 Hz, 4H, H-1'), 7.20 – 7.14 (m, 6H, H-2'/, H-4), 6.66 (s, 2H, 3-OH), 6.58 (dd, *J* = 8.5, 2.7 Hz, 2H, H-2), 6.52 (d, *J* = 2.7 Hz, 2H, H-1), 3.52 (s, 2H, 17-OH), 2.86 – 2.75 (m, 4H), 2.48 – 2.33 (m, 4H), 2.15 – 1.99 (m, 6H), 1.90 – 1.79 (m, 6H), 1.58 – 1.31 (m, 10H), 0.94 (s, 6H, H-18). **^{13}C-NMR** δ (CD_3CN, 100 MHz): 159.14, 156.51 (C-1'), 155.60, 153.47, 148.32, 139.08 (C-3'), 137.34, 133.45 (C-11'), 132.65, 128.94 (C-10'), 128.50, 127.45, 126.36, 125.57, 122.48 (C-7'), 116.06 (C-4), 113.65 (C-2), 97.59, 85.27 (C-19), 80.81 (C-20), 50.92,

View Article Online
DOI: 10.1039/D3DT03480A

48.72, 44.71, 40.61, 39.97, 34.21, 30.35, 28.19, 27.50, 23.71, 13.47 (C-18). **MS** (ESI-TOF$^+$) *m/z* calcd. for $C_{82}H_{74}N_6O_4Ru$ [*M*-2xPF_6]$^{2+}$: 654.24. Found: 654.17.

Computational methods

The molecular structure of the investigated ruthenium nitrosyl complexes was fully optimized using the Gaussian-09 program package[66] within the framework of the Density Functional Theory (DFT). The double-ζ basis set 6-31G* was used for all atoms except the heavy ruthenium atom, for which the LANL2DZ basis set was applied to account for relativistic effects.[67-69] To be consistent with our previous reports on RuNO complexes,[53, 70] and in agreement with a previous investigation of ruthenium-nitrosyl by Mascharak,[71] we have selected the hybrid functional B3PW91 for the optimization. B3PW91 has been shown to outperform other hybrid functionals (*e.g.* B3LYP) and pure functionals (*e.g.* PW91) in numerous cases of ruthenium complexes, especially when back bonding ligands (like NO) are present.[71-72] The vibrational analyses were performed at the same level to verify that the stationary points correspond to minima on the potential energy surfaces, computed frequencies were scaled by a 0.9573 scaling factor as described elsewhere.[56] The UV-visible electronic spectra were then computed at the CAM-B3LYP/6-31G* level, which was selected for its good efficiency to reproduce experimental transition energies within a maximum uncertainty of 0.3 eV. Solvent effects were included by using the polarizable continuum model (PCM) implemented in Gaussian09 for water (ε=78.355) for **[EE-Phtpy-RuNO]**$^+$ and **[Phtpy-RuNO]**$^+$ and acetonitrile (ε=35.688) for **[*cis*-4a-b]**$^+$ and **[*trans*-4a-b]**$^+$. An overall tendency towards higher energies computed by TD-DFT is observed in any case for the high intensity transitions with values around 2000 cm^{-1}; these differences were found acceptable considering the large molecular sizes, heavy ruthenium atoms, and sizeable charge transfer.[73]

Photochemistry

Kinetic studies on the photolysis reactions A → B were carried out with a diode array Hewlett Packart 8454A spectrophotometer. The optical fiber was fixed laterally from the cuvette. Absorption spectra were taken after each minute, in fast scan mode. The UV-visible spectra were recorded under irradiation realized with a Muller reactor device equipped with a cooling water filter and monochromatic LEDs. The light intensity was determined by using a power-meter from Thorlabs (PM100D). The sample solutions were placed in a quartz cuvette of 1 cm path-length stirred continuously (l_r = 1). The temperature was maintained at 25 °C during the whole experiment. The quantum yield (ϕ_{AB}^{λ}) was determined by the program Sa3.3 written by D. Lavabre and V. Pimienta.[74-75] It allows the resolution of the differential equation with the rate of the photochemical processes r_A expressed as follows:

$$r_A = -\frac{d[A]}{dt} = \frac{d[B]}{dt} \quad \text{with} \quad r_A = -\phi_{AB}^{\lambda} \varepsilon_A^{\lambda}[A]\, l_r\, I_0^{\lambda} F^{\lambda} \qquad (2)$$

View Article Online
DOI: 10.1039/D3DT03480A

In this equation, F^{λ} is the photokinetic factor, l_r is the photochemical reactor irradiation optical path, ϕ_{AB}^{λ} is the quantum yield of the photochemical reaction of *A* transformed in *B* at the irradiation wavelength λ, I_0^{λ} is the intensity of the irradiation photon flux at λ (in mol L^{-1} s^{-1}).

The photokinetic factor F^{λ} is expressed as $F^{\lambda} = (1 - 10^{-Abs^{\lambda}})/Abs^{\lambda}$, in which Abs^{λ} is the total absorbance of the absorbing species at the irradiation wavelength λ ($Abs^{\lambda} = (\varepsilon_A \cdot [A] + \varepsilon_B \cdot [B]) \cdot l_r$, ε (in mol^{-1} L cm^{-1}) is the molar extinction coefficient of the ruthenium nitrosyl complex. The equation was fitted with the experimental data Abs = *f*(t) and 2 parameters ϕ_{AB}^{λ} and ε_B (ε_B is the molar extinction coefficient measured at the end of the reaction). λ_{obs} was chosen to correspond to a large difference between molar extinction coefficient at the initial and final time of the photochemical reaction. Simulation and optimization procedures were performed by using numerical integration and a non-linear minimization algorithm for the fitting of the model to the experimental data.

Partition coefficient (logP) measurements

Measurements were performed following as described elsewhere[76] with minor adaptations. Briefly, fresh samples of complexes **Phtpy-RuNO** and **EE-Phtpy-RuNO** were prepared from each complex at $4x10^{-5}$ M in water (0,5 % DMSO) stirred 72 hours at room temperature. An equivalent amount of *n*-octanol was added and the mixture was vortexed twice at 2000 rpm for 60 sec, with a pause of 30 sec in between. UV-Visible spectra for each layer were recorded taking an appropriate aliquot and diluting with methanol and either *n*-octanol or water in order to keep a constant water/methanol/1-octanol ratio along all the measurements. Experiments for each complex were performed by triplicate to ensure reproducibility.

EPR experiments

Electron paramagnetic resonance (EPR) spectra were collected on a Bruker ESP 500E (X band) spectrometer. Nmethyl- D-glucamine dithiocarbamate previously synthesized[77] reacted with Mohr salts to get [$Fe(MGD)_2$]. 90 µL of 1 mM of Ru(NO) complexes in acetonitrile (***cis*-4a-b**/***trans*-4a-b**) or water (+0.5 % DMSO, **EE-Phtpy-RuNO**/**Phtpy-RuNO**) were mixed with 10 µL of an aqueous solution of 20 mM [$Fe(MGD)_2$] and injected into quartz capillaries. Samples were irradiated directly in the EPR cavity using a λ = 365 nm LED.

Cell culture

Primary dermal fibroblasts were isolated from 3-year old foreskin commercially bought (Icelltis) after posthectomy as previously described.[78-79] Cells were tested negative for mycoplasma using MycoAlert mycoplasma detection kit (Lonza) all along the experiments. Dermal fibroblasts were grown in Dulbecco's Modified Eagles Medium (Gibco-Invitrogen) containing phenol red, 4.5 $g.L^{-1}$ glucose, Glutamax, and 1mM pyruvate, supplemented with 10 % (v/v) of heat inactivated fetal calf serum, 100 U/ml penicillin, and 100 $\mu g.mL^{-1}$ streptomycin. Cells were maintained at 37°C in a humidified atmosphere containing 5 % CO_2 and cell culture media were changed three times a week.

Quantification by inductively coupled plasma mass spectrometry (ICP-MS) of Ru-NO complexes cell penetration

View Article Online
DOI: 10.1039/D3DT03480A

600,000 fibroblasts were seeded in a 75cm² flask and let grown for seven days, until reaching confluence. On the day of the experiment, cells were incubated for 3h at 37°C with 10ml of cell culture medium containing 10 µM of **Phtpy-RuNO**, 10 µM of **EE-Phtpy-RuNO**, or 0.5% DMSO as control condition. After incubation, cells were washed twice with 5ml of phosphate buffer saline (PBS), trypsinized, counted (3 million of cell per pellet) and centrifuged. Dried cell pellets were kept at 4°C until being analyzed by ICP-MS for Ru quantification by a private company (GLINCs, Villeurbanne, France). Briefly, cell pellets were lysed in acidic condition (0.7% 1-butanol / 0.1% Triton X100 / 20% HNO_3%), sonicated at 80°C for 2h and diluted ten times in HNO_3 0.25% before being analyzed on Nexion 2000 (Perkin Elmer).

ACKNLOWLEDGMENTS

Authors thank Dr. Patricia Vicendo for fruitful discussions. P.L.-V. and Y.X. acknowledge support from the French National Research Agency under programs ANR-18-CE29-0012 and ANR-20-CE18-0032, respectively. N.F. acknowledges support from PAIP and PAPIIT (IN200422).

REFERENCES

1. World Health Organization. "Cancer" 2022. Available from: https://www.who.int/news-room/fact-sheets/detail/cancer. Consulted: 22/Sep/2023.
2. Anand, U.; Dey, A.; Chandel, A. K. S.; Sanyal, R.; Mishra, A.; Pandey, D. K.; De Falco, V.; Upadhyay, A.; Kandimalla, R.; Chaudhary, A.; Dhanjal, J. K.; Dewanjee, S.; Vallamkondu, J.; Pérez de la Lastra, J. M., Cancer chemotherapy and beyond: Current status, drug candidates, associated risks and progress in targeted therapeutics. *Genes Dis.* **2023,** *10* (4), 1367-1401.
3. Zhong, L.; Li, Y.; Xiong, L.; Wang, W.; Wu, M.; Yuan, T.; Yang, W.; Tian, C.; Miao, Z.; Wang, T.; Yang, S., Small molecules in targeted cancer therapy: advances, challenges, and future perspectives. *Signal Transduct. Target. Ther.* **2021,** *6* (1), 201.
4. Lu, Y.; Zhu, D.; Le, Q.; Wang, Y.; Wang, W., Ruthenium-based antitumor drugs and delivery systems from monotherapy to combination therapy. *Nanoscale* **2022,** *14* (44), 16339-16375.
5. Manzari, M. T.; Shamay, Y.; Kiguchi, H.; Rosen, N.; Scaltriti, M.; Heller, D. A., Targeted drug delivery strategies for precision medicines. *Nat. Rev. Mater.* **2021,** *6* (4), 351-370.
6. Poynton, F. E.; Bright, S. A.; Blasco, S.; Williams, D. C.; Kelly, J. M.; Gunnlaugsson, T., The development of ruthenium(ii) polypyridyl complexes and conjugates for in vitro cellular and in vivo applications. *Chem. Soc. Rev.* **2017,** *46* (24), 7706-7756.
7. Lipinski, C. A.; Lombardo, F.; Dominy, B. W.; Feeney, P. J., Experimental and computational approaches to estimate solubility and permeability in drug discovery and development settings. *Adv. Drug Del. Rev.* **1997,** *23* (1), 3-25.
8. Ghose, A. K.; Viswanadhan, V. N.; Wendoloski, J. J., A Knowledge-Based Approach in Designing Combinatorial or Medicinal Chemistry Libraries for Drug Discovery. 1. A Qualitative and Quantitative Characterization of Known Drug Databases. *J. Comb. Chem.* **1999,** *1* (1), 55-68.
9. Fichert, T.; Yazdanian, M.; Proudfoot, J. R., A structure–Permeability study of small drug-like molecules. *Bioorg. Med. Chem. Lett.* **2003,** *13* (4), 719-722.
10. Vega-Vásquez, P.; Mosier, N. S.; Irudayaraj, J., Nanoscale Drug Delivery Systems: From Medicine to Agriculture. *Front. Bioeng. Biotechnol.* **2020,** *8*.

View Article Online
DOI: 10.1039/D3DT03480A

11. Saha, P.; Descôteaux, C.; Brasseur, K.; Fortin, S.; Leblanc, V.; Parent, S.; Asselin, É.; Bérubé, G., Synthesis, antiproliferative activity and estrogen receptor α affinity of novel estradiol-linked platinum(II) complex analogs to carboplatin and oxaliplatin. Potential vector complexes to target estrogen-dependent tissues. *Eur. J. Med. Chem.* **2012,** *48*, 385-390.
12. Mukhopadhyay, S.; Barnés, C. M.; Haskel, A.; Short, S. M.; Barnes, K. R.; Lippard, S. J., Conjugated Platinum(IV)−Peptide Complexes for Targeting Angiogenic Tumor Vasculature. *Bioconjug. Chem.* **2008,** *19* (1), 39-49.
13. Schmid, S. L., A nostalgic look back 40 years after the discovery of receptor-mediated endocytosis. *Mol. Biol. Cell* **2019,** *30* (1), 1-3.
14. Basu, S. K., Receptor-mediated endocytosis: An overview of a dynamic process. *J. Biosci.* **1984,** *6* (4), 535-542.
15. Aronov, O.; Horowitz, A. T.; Gabizon, A.; Gibson, D., Folate-Targeted PEG as a Potential Carrier for Carboplatin Analogs. Synthesis and in Vitro Studies. *Bioconjug. Chem.* **2003,** *14* (3), 563-574.
16. Ouyang, X.; Wang, X.; Kraatz, H.-B.; Ahmadi, S.; Gao, J.; Lv, Y.; Sun, X.; Huang, Y., A Trojan horse biomimetic delivery strategy using mesenchymal stem cells for PDT/PTT therapy against lung melanoma metastasis. *Biomater. Sci.* **2020,** *8* (4), 1160-1170.
17. Pardridge, W. M., Molecular Trojan horses for blood–brain barrier drug delivery. *Curr. Opin. Pharmacol.* **2006,** *6* (5), 494-500.
18. Jackson, A.; Davis, J.; Pither, R. J.; Rodger, A.; Hannon, M. J., Estrogen-Derived Steroidal Metal Complexes: Agents for Cellular Delivery of Metal Centers to Estrogen Receptor-Positive Cells. *Inorg. Chem.* **2001,** *40* (16), 3964-3973.
19. Liang, Z.; Liu, L.; Zhou, Y.; Liu, W.; Lu, Y., Research Progress on Bioactive Metal Complexes against ER-Positive Advanced Breast Cancer. *J. Med. Chem.* **2023,** *66* (4), 2235-2256.
20. Benson, S.; de Moliner, F.; Fernandez, A.; Kuru, E.; Asiimwe, N. L.; Lee, J.-S.; Hamilton, L.; Sieger, D.; Bravo, I. R.; Elliot, A. M.; Feng, Y.; Vendrell, M., Photoactivatable metabolic warheads enable precise and safe ablation of target cells in vivo. *Nat. Commun.* **2021,** *12* (1), 2369.
21. Gagnon, V.; St-Germain, M.-È.; Descôteaux, C.; Provencher-Mandeville, J.; Parent, S.; Mandal, S. K.; Asselin, E.; Bérubé, G., Biological evaluation of novel estrogen-platinum(II) hybrid molecules on uterine and ovarian cancers—molecular modeling studies. *Bioorg. Med. Chem. Lett.* **2004,** *14* (23), 5919-5924.
22. Mari, C.; Pierroz, V.; Leonidova, A.; Ferrari, S.; Gasser, G., Towards Selective Light-Activated RuII-Based Prodrug Candidates. *Eur. J. Inorg. Chem.* **2015,** *2015* (23), 3879-3891.
23. Dunkel, P.; Ilaš, J., Targeted Cancer Therapy Using Compounds Activated by Light. *Cancers (Basel)* **2021,** *13* (13), 3237.
24. Martínez-Alonso, M.; Gasser, G., Ruthenium polypyridyl complex-containing bioconjugates. *Coord. Chem. Rev.* **2021,** *434*, 213736.
25. Silva, M. J. S. A.; Vinck, R.; Wang, Y.; Saubaméa, B.; Tharaud, M.; Dominguez-Jurado, E.; Karges, J.; Gois, P. M. P.; Gasser, G., Towards Selective Delivery of a Ruthenium(II) Polypyridyl Complex-Containing Bombesin Conjugate into Cancer Cells. *ChemBioChem* **2023,** *24* (4), e202200647.
26. Farrer, N. J.; Salassa, L.; Sadler, P. J., Photoactivated chemotherapy (PACT): the potential of excited-state d-block metals in medicine. *Dalton Trans.* **2009,** (48), 10690-10701.
27. Bonnet, S., Why develop photoactivated chemotherapy? *Dalton Trans.* **2018,** *47* (31), 10330-10343.

View Article Online
DOI: 10.1039/D3DT03480A

28. Yue, X.; Guo, T.; Zhang, H.; Wang, B.; Lan, M.; Song, X., An estradiol-functionalized red-emissive photosensitizer for enhanced and precise photodynamic therapy of breast cancers. *Chem. Commun.* **2023,** *59* (46), 7060-7063.
29. Viola, G.; Dall'Acqua, F., Photosensitization of Biomolecules by Phenothiazine Derivatives. *Curr. Drug Targets* **2006,** *7* (9), 1135-1154.
30. Mfouo-Tynga, I. S.; Dias, L. D.; Inada, N. M.; Kurachi, C., Features of third generation photosensitizers used in anticancer photodynamic therapy: Review. *Photodiagnosis Photodyn. Ther.* **2021,** *34*, 102091.
31. Gunaydin, G.; Gedik, M. E.; Ayan, S., Photodynamic Therapy for the Treatment and Diagnosis of Cancer–A Review of the Current Clinical Status. *Front. Chem.* **2021,** *9*.
32. Thomas, D. D.; Ridnour, L. A.; Isenberg, J. S.; Flores-Santana, W.; Switzer, C. H.; Donzelli, S.; Hussain, P.; Vecoli, C.; Paolocci, N.; Ambs, S.; Colton, C. A.; Harris, C. C.; Roberts, D. D.; Wink, D. A., The chemical biology of nitric oxide: Implications in cellular signaling. *Free Radic. Biol. Med.* **2008,** *45* (1), 18-31.
33. Girotti, A. W., Tumor-generated nitric oxide as an antagonist of photodynamic therapy. *Photochem. Photobiol. Sci.* **2015,** *14* (8), 1425-1432.
34. Lacroix, P. G.; Malfant, I.; Labra-Vázquez, P.; Fárfan, N.; Ramos-Ortiz, G., Two-photon absorption-based delivery of nitric oxide from ruthenium nitrosyl complexes. *Dalton Trans.* **2022,** *51* (39), 14833-14841.
35. Juarez-Martinez, Y.; Labra-Vázquez, P.; Enríquez-Cabrera, A.; Leon-Rojas, A. F.; Martínez-Bourget, D.; Lacroix, P. G.; Tassé, M.; Mallet-Ladeira, S.; Farfán, N.; Santillan, R.; Ramos-Ortiz, G.; Malval, J.-P.; Malfant, I., Bimetallic Ruthenium Nitrosyl Complexes with Enhanced Two-Photon Absorption Properties for Nitric Oxide Delivery. *Chem. Eur. J.* **2022,** *28* (62), e202201692.
36. Bocé, M.; Tassé, M.; Mallet-Ladeira, S.; Pillet, F.; Da Silva, C.; Vicendo, P.; Lacroix, P. G.; Malfant, I.; Rols, M.-P., Effect of trans(NO, OH)-[RuFT(Cl)(OH)NO](PF6) ruthenium nitrosyl complex on methicillin-resistant Staphylococcus epidermidis. *Sci. Rep.* **2019,** *9* (1), 4867.
37. Labra-Vázquez, P.; Bocé, M.; Tassé, M.; Mallet-Ladeira, S.; Lacroix, P. G.; Farfán, N.; Malfant, I., Chemical and photochemical behavior of ruthenium nitrosyl complexes with terpyridine ligands in aqueous media. *Dalton Trans.* **2020,** *49* (10), 3138-3154.
38. Keam, S. J.; Wagstaff, A. J., Ethinylestradiol/Drospirenone. *Treat. Endocrinol.* **2003,** *2* (1), 49-70.
39. Bansal, R.; Suryan, A., A Comprehensive Review on Steroidal Bioconjugates as Promising Leads in Drug Discovery. *ACS Bio. & Med. Chem. Au* **2022,** *2* (4), 340-369.
40. W.R. Miller, Aromatase inhibitors and breast cancer, *Cancer Treat. Rev.* **1997**, *23* (3), 171-187
41. Arnal, J.-F.; Lenfant, F.; Metivier, R.; Flouriot, G.; Henrion, D.; Adlanmerini, M.; Fontaine, C.; Gourdy, P.; Chambon, P.; Katzenellenbogen, B.; Katzenellenbogen, J., Membrane and Nuclear Estrogen Receptor Alpha Actions: From Tissue Specificity to Medical Implications. *Physiol. Rev.* **2017,** *97* (3), 1045-1087.
42. Pietras, R. J.; Szego, C. M., Specific internalization of estrogen and binding to nuclear matrix in isolated uterine cells. *Biochem. Biophys. Res. Commun.* **1984,** *123* (1), 84-91.
43. Acconcia, F.; Marino, M., The effects of 17b-estradiol in cancer are mediated by estrogen receptor signaling at the plasma membrane. *Front. Physiol.* **2011,** *2*.

View Article Online
DOI: 10.1039/D3DT03480A

44. Haczynski, J.; Tarkowski, R.; Jarzabek, K.; Slomczynska, M.; Wolczynski, S.; Magoffin, D. A.; Jakowicki, J. A.; Jakimiuk, A. J., Human cultured skin fibroblasts express estrogen receptor α and β. *Int. J. Mol. Med.* **2002,** *10* (2), 149-153.
45. Gabano, E.; Cassino, C.; Bonetti, S.; Prandi, C.; Colangelo, D.; Ghiglia, A.; Osella, D., Synthesis and characterisation of estrogenic carriers for cytotoxic Pt(ii) fragments: biological activity of the resulting complexes. *Org. Biomol. Chem.* **2005,** *3* (19), 3531-3539.
46. Damodaran, S.; Hortobagyi, G. N., Estrogen Receptor: A Paradigm for Targeted Therapy. *Cancer Res.* **2021,** *81* (21), 5396-5398.
47. Ott, I.; Gust, R., Preclinical and Clinical Studies on the Use of Platinum Complexes for Breast Cancer Treatment. *Anticancer Agents Med. Chem.* **2007,** *7* (1), 95-110.
48. Amabilino, S.; Tasse, M.; Lacroix, P. G.; Mallet-Ladeira, S.; Pimienta, V.; Akl, J.; Sasaki, I.; Malfant, I., Photorelease of nitric oxide (NO) on ruthenium nitrosyl complexes with phenyl substituted terpyridines. *New J. Chem.* **2017,** *41* (15), 7371-7383.
49. Zhang, X.; Zuo, Z.; Tang, J.; Wang, K.; Wang, C.; Chen, W.; Li, C.; Xu, W.; Xiong, X.; Yuntai, K.; Huang, J.; Lan, X.; Zhou, H.-B., Design, synthesis and biological evaluation of novel estrogen-derived steroid metal complexes. *Bioorg. Med. Chem. Lett.* **2013,** *23* (13), 3793-3797.
50. Wang, J.; Hanan, G. S., A Facile Route to Sterically Hindered and Non-Hindered 4′-Aryl-2,2′:6′,2″-Terpyridines. *Synlett* **2005,** *2005* (08), 1251-1254.
51. Bocé, M.; Tassé, M.; Mallet-Ladeira, S.; Pillet, F.; Da Silva, C.; Vicendo, P.; Lacroix, P. G.; Malfant, I.; Rols, M.-P., Author Correction: Effect of trans(NO, OH)-[RuFT(Cl)(OH)NO](PF6) ruthenium nitrosyl complex on methicillin-resistant Staphylococcus epidermidis. *Sci. Rep.* **2019,** *9* (1), 15162.
52. Hansch, C.; Leo, A.; Taft, R. W., A survey of Hammett substituent constants and resonance and field parameters. *Chem. Rev.* **1991,** *91* (2), 165-195.
53. Akl, J.; Sasaki, I.; Lacroix, P. G.; Malfant, I.; Mallet-Ladeira, S.; Vicendo, P.; Farfán, N.; Santillan, R., Comparative photo-release of nitric oxide from isomers of substituted terpyridinenitrosylruthenium(ii) complexes: experimental and computational investigations. *Dalton Trans.* **2014,** *43* (33), 12721-12733.
54. Giri, B.; Saini, T.; Kumbhakar, S.; Selvan K, K.; Muley, A.; Misra, A.; Maji, S., Near-IR light-induced photorelease of nitric oxide (NO) on ruthenium nitrosyl complexes: formation, reactivity, and biological effects. *Dalton Trans.* **2020,** *49* (31), 10772-10785.
55. Giri, B.; Kumbhakar, S.; Selvan K, K.; Muley, A.; Maji, S., Ruthenium nitrosyl complexes with the molecular framework [RuII(dmdptz)(bpy)(NO)]n+ (dmdptz: N,N-dimethyl-4,6-di(pyridin-2-yl)-1,3,5-triazin-2-amine and bpy: 2,2′-bipyridine). Electronic structure, reactivity aspects, photorelease, and scavenging of NO. *New J. Chem.* **2020,** *44* (43), 18732-18744.
56. Scott, A. P.; Radom, L., Harmonic Vibrational Frequencies: An Evaluation of Hartree−Fock, Møller−Plesset, Quadratic Configuration Interaction, Density Functional Theory, and Semiempirical Scale Factors. *J. Phys. Chem.* **1996,** *100* (41), 16502-16513.
57. Enemark, J. H.; Feltham, R. D., Principles of structure, bonding, and reactivity for metal nitrosyl complexes. *Coord. Chem. Rev.* **1974,** *13* (4), 339-406.
58. Ramírez-Lozano, C. M.; Eugenia Ochoa, M.; Labra-Vázquez, P.; Farfán, N.; Santillan, R., Synthesis, crystal structure and computational studies of new steroidal hemisuccinyl ester derivatives. *J. Mol. Struct.* **2023,** *1272*, 134191.

View Article Online
DOI: 10.1039/D3DT03480A

59. Guguta, C.; Eeuwijk, I.; Smits, J. M. M.; de Gelder, R., Structural Diversity of Ethinyl Estradiol Solvates. *Cryst. Growth Des.* **2008,** *8* (3), 823-831.
60. Labra-Vázquez, P.; Ochoa, M. E.; Alfonso-Herrera, L. A.; Vera, M. A.; Farfán, N.; Santillan, R., A Steroidal Molecular Rotor with Fast Solid-State Dynamics Obtained by Crystal Engineering: Role of the Polarity of the Stator. *Eur. J. Org. Chem.* **2022,** *2022* (38), e202200351.
61. Tsikas, D., Analysis of nitrite and nitrate in biological fluids by assays based on the Griess reaction: Appraisal of the Griess reaction in the l-arginine/nitric oxide area of research. *J. Chromatogr. B* **2007,** *851* (1), 51-70.
62. Liu, J.; Duan, Q.; Wang, J.; Song, Z.; Qiao, X.; Wang, H., Photocontrolled nitric oxide release from two nitrosylruthenium isomer complexes and their potential biomedical applications. *J. Biomed. Opt.* **2015,** *20* (1), 015004.
63. Sheldrick, G., SHELXT - Integrated space-group and crystal-structure determination. *Acta Crystallogr. A* **2015,** *71* (1), 3-8.
64. Betteridge, P. W.; Carruthers, J. R.; Cooper, R. I.; Prout, K.; Watkin, D. J., CRYSTALS version 12: software for guided crystal structure analysis. *J. Appl. Crystallogr.* **2003,** *36* (6), 1487.
65. Spek, A., PLATON SQUEEZE: a tool for the calculation of the disordered solvent contribution to the calculated structure factors. *Acta Crystallogr. C* **2015,** *71* (1), 9-18.
66. Gaussian 09, Revision D.01, M. J. Frisch, G. W. Trucks, H. B. Schlegel, G. E. Scuseria, M. A. Robb, J. R. Cheeseman, G. Scalmani, V. Barone, B. Mennucci, G. A. Petersson, H. Nakatsuji, M. Caricato, X. Li, H. P. Hratchian, A. F. Izmaylov, J. Bloino, G. Zheng, J. L. Sonnenberg, M. Hada, M. Ehara, K. Toyota, R. Fukuda, J. Hasegawa, M. Ishida, T. Nakajima, Y. Honda, O. Kitao, H. Nakai, T. Vreven, J. A. Montgomery, Jr., J. E. Peralta, F. Ogliaro, M. Bearpark, J. J. Heyd, E. Brothers, K. N. Kudin, V. N. Staroverov, T. Keith, R. Kobayashi, J. Normand, K. Raghavachari, A. Rendell, J. C. Burant, S. S. Iyengar, J. Tomasi, M. Cossi, N. Rega, J. M. Millam, M. Klene, J. E. Knox, J. B. Cross, V. Bakken, C. Adamo, J. Jaramillo, R. Gomperts, R. E. Stratmann, O. Yazyev, A. J. Austin, R. Cammi, C. Pomelli, J. W. Ochterski, R. L. Martin, K. Morokuma, V. G. Zakrzewski, G. A. Voth, P. Salvador, J. J. Dannenberg, S. Dapprich, A. D. Daniels, O. Farkas, J. B. Foresman, J. V. Ortiz, J. Cioslowski, D. J. Fox, Gaussian, Inc., Wallingford CT, 2013.
67. Hay, P. J.; Wadt, W. R., Ab initio effective core potentials for molecular calculations. Potentials for the transition metal atoms Sc to Hg. *J. Chem. Phys.* **1985,** *82* (1), 270-283.
68. Wadt, W. R.; Hay, P. J., Ab initio effective core potentials for molecular calculations. Potentials for main group elements Na to Bi. *J. Chem. Phys.* **1985,** *82* (1), 284-298.
69. Hay, P. J.; Wadt, W. R., Ab initio effective core potentials for molecular calculations. Potentials for K to Au including the outermost core orbitals. *J. Chem. Phys.* **1985,** *82* (1), 299-310.
70. Enriquez-Cabrera, A.; Sasaki, I.; Bukhanko, V.; Tassé, M.; Mallet-Ladeira, S.; Lacroix, P. G.; Barba-Barba, R. M.; Ramos-Ortiz, G.; Farfán, N.; Voitenko, Z.; Malfant, I., Replacing Two Chlorido Ligands by a Bipyridine Ligand in Ruthenium Nitrosyl Complexes with NO-Release Capabilities: A Comparative Study. *Eur. J. Inorg. Chem.* **2017,** *2017* (11), 1446-1456.
71. Rose, M. J.; Mascharak, P. K., Photosensitization of Ruthenium Nitrosyls to Red Light with an Isoelectronic Series of Heavy-Atom Chromophores: Experimental and Density Functional Theory Studies on the Effects of O-, S- and Se-Substituted Coordinated Dyes. *Inorg. Chem.* **2009,** *48* (14), 6904-6917.
72. Hirva, P.; Haukka, M.; Jakonen, M.; Moreno, M. A., DFT tests for group 8 transition metal carbonyl complexes. *J. Mol. Model.* **2008,** *14* (3), 171-181.

View Article Online
DOI: 10.1039/D3DT03480A

73. Laurent, A. D.; Jacquemin, D., TD-DFT benchmarks: A review. *Int. J. Quantum Chem.* **2013,** *113* (17), 2019-2039.
74. Pimienta, V.; Frouté, C.; Deniel, M. H.; Lavabre D.; Guglielmetti, R.; Micheau, J. C., Kinetic modelling of the photochromism and photodegradation of a spiro[indoline-naphthoxazine]. *J. Photochem. Photobiol. A*, **1999**, *22*, 199.
75. Sa3.3 software can be downloaded at http://cinet.chim.pagesperso-orange.fr/
76. Rothbard, J. B.; Jessop, T. C.; Lewis, R. S.; Murray, B. A.; Wender, P. A., Role of Membrane Potential and Hydrogen Bonding in the Mechanism of Translocation of Guanidinium-Rich Peptides into Cells. *J. Am. Chem.l Soc.* **2004,** *126* (31), 9506-9507.
77. Shinobu, L. A.; Jones, S. G.; Jones, M. M., Sodium N-Methyl-D-glucamine Dithiocarbamate and Cadmium Intoxication. *Acta Pharmacol. Toxicol. (Copenh.)* **1984,** *54* (3), 189-194.
78. Gouarderes, S.; Doumard, L.; Vicendo, P.; Mingotaud, A.-F.; Rols, M.-P.; Gibot, L., Electroporation does not affect human dermal fibroblast proliferation and migration properties directly but indirectly via the secretome. *Bioelectrochemistry* **2020,** *134*, 107531.
79. Gouarderes, S.; Ober, C.; Doumard, L.; Dandurand, J.; Vicendo, P.; Fourquaux, I.; Golberg, A.; Samouillan, V.; Gibot, L., Pulsed Electric Fields Induce Extracellular Matrix Remodeling through Matrix Metalloproteinases Activation and Decreased Collagen Production. *J. Invest. Dermatol.* **2022,** *142* (5), 1326-1337.e9.